nature chemical biology

ARTICLES

Synthetic partial agonists reveal key steps in IP_3 receptor activation

Ana M Rossi[1,4], Andrew M Riley[2,4], Stephen C Tovey[1], Taufiq Rahman[1], Olivier Dellis[1], Emily J A Taylor[1], Valery G Veresov[3], Barry V L Potter[2] & Colin W Taylor[1]

Inositol 1,4,5-trisphosphate receptors (IP_3Rs) are ubiquitous intracellular Ca^{2+} channels. IP_3 binding to the IP_3-binding core (IBC) near the N terminus initiates conformational changes that lead to opening of a pore. The mechanisms underlying this process are unresolved. We synthesized 2-O–modified IP_3 analogs that are partial agonists of IP_3R. These are similar to IP_3 in their interactions with the IBC, but they are less effective than IP_3 in rearranging the relationship between the IBC and the N-terminal suppressor domain (SD), and they open the channel at slower rates. IP_3R with a mutation in the SD occupying a position similar to the 2-O substituent of the partial agonists has a reduced open probability that is similar for full and partial agonists. Bulky or charged substituents from either the ligand or the SD therefore block obligatory coupling of the IBC and the SD. Analysis of ΔG for ligand binding shows that IP_3 is recognized by the IBC and conformational changes then propagate entirely via the SD to the pore.

IP_3Rs are ligand-gated channels. They are expressed in most animal cells and mediate release of Ca^{2+} from the endoplasmic reticulum in response to the many stimuli that evoke IP_3 formation. IP_3Rs are tetrameric, and each subunit of about 2,700 residues has an IP_3 binding site near the N terminus and six transmembrane domains (TMDs) toward the C terminus (**Fig. 1a**)[1]. The pore is formed by the last pair of TMDs and the intervening loop, the pore loop ("P-loop"), from all four subunits[1]. The structure of the pore is predicted to be broadly similar to the pores of other tetrameric P-loop channels, such as bacterial K^+ channels, for which high-resolution structures are available[2]. IP_3 binds to a discrete part of the IP_3R: the IBC (residues 224–604, **Fig. 1a**)[3]. Although the extreme N terminus (residues 1–223) is not required for IP_3 binding, it decreases the affinity for IP_3 and has therefore been called the suppressor domain (SD)[4]. The SD is thought to be required for channel gating because IP_3 binds to IP_3R without an SD, but it no longer opens the pore[4,5]. However, the links between IP_3 binding and gating are not understood, and we do not have a structure of the entire IP_3R at sufficient resolution to provide insight into these gating mechanisms[1,6].

Activation of ligand-gated ion channels begins with agonist binding to a stable closed state and proceeds via many short-lived intermediates to a state in which the pore is open[7]. This activation may proceed entirely through a sequence of incremental changes in the receptor[8], or it may be dominated by a single concerted transition between two stable conformations[9]. Agonists differ in the strength of their binding (affinity) and in their ability to drive the receptor to its open state (efficacy)[10]. A ligand with reduced efficacy must occupy more receptors than a full agonist to evoke the same cellular response. Such partial agonists, by occupying receptors, diminish the response to a full agonist[11]. Partial agonists are particularly useful for exploring the mechanisms of receptor activation because they lie between full agonists and antagonists in their ability to activate receptors[7,10]. This is true for all receptors, but ligand-gated ion channels are uniquely amenable to such analyses because single-channel recording allows key conformational changes of single receptors to be determined with outstanding temporal resolution[7].

For these ligand-gated ion channels, full and partial agonists may differ in the frequency with which they cause the receptor to visit the fully active open state, or they may stabilize different open states that mediate lesser ion fluxes. In both cases, a partial agonist evokes lesser activation. Two subtypes of ionotropic glutamate receptors (iGluRs) illustrate the distinction. These receptors mediate most excitatory neurotransmission in the brain, and the structural basis of their efficacy has been more thoroughly explored than that of any other receptor[12,13]. For the α-amino-3-hydroxyl-5-methyl-4-isoxazole-propionate (AMPA) subtype of iGluR, a series of partial agonists that differ from each other by only a single atom close the clam-like binding site to varying degrees, but less completely than do full agonists. Partial agonists thereby preferentially open the pore to states with lesser conductance[12]. For full and partial agonists of the *N*-methyl-D-aspartic acid (NMDA) subtype of iGluR, the conformational changes in the binding site are more subtly different. They cause similar closure of the clam, and they fully open the pore, but the conformational changes proceed more slowly for partial agonists[14,15].

Affinity and efficacy are distinguishable, but the two properties are not independent because energy provided by agonist binding drives

[1]Department of Pharmacology, University of Cambridge, Cambridge, UK. [2]Wolfson Laboratory of Medicinal Chemistry, Department of Pharmacy and Pharmacology, University of Bath, Claverton Down, Bath, UK. [3]Department of Cell Biophysics, Institute of Biophysics and Cell Engineering, National Academy of Sciences of Belarus, Minsk, Belarus. [4]These authors contributed equally to this work. Correspondence should be addressed to C.W.T. (cwt1000@cam.ac.uk) or B.V.L.P. (b.v.l.potter@bath.ac.uk).

Received 9 January; accepted 22 May; published online 9 August 2009; doi:10.1038/nchembio.195

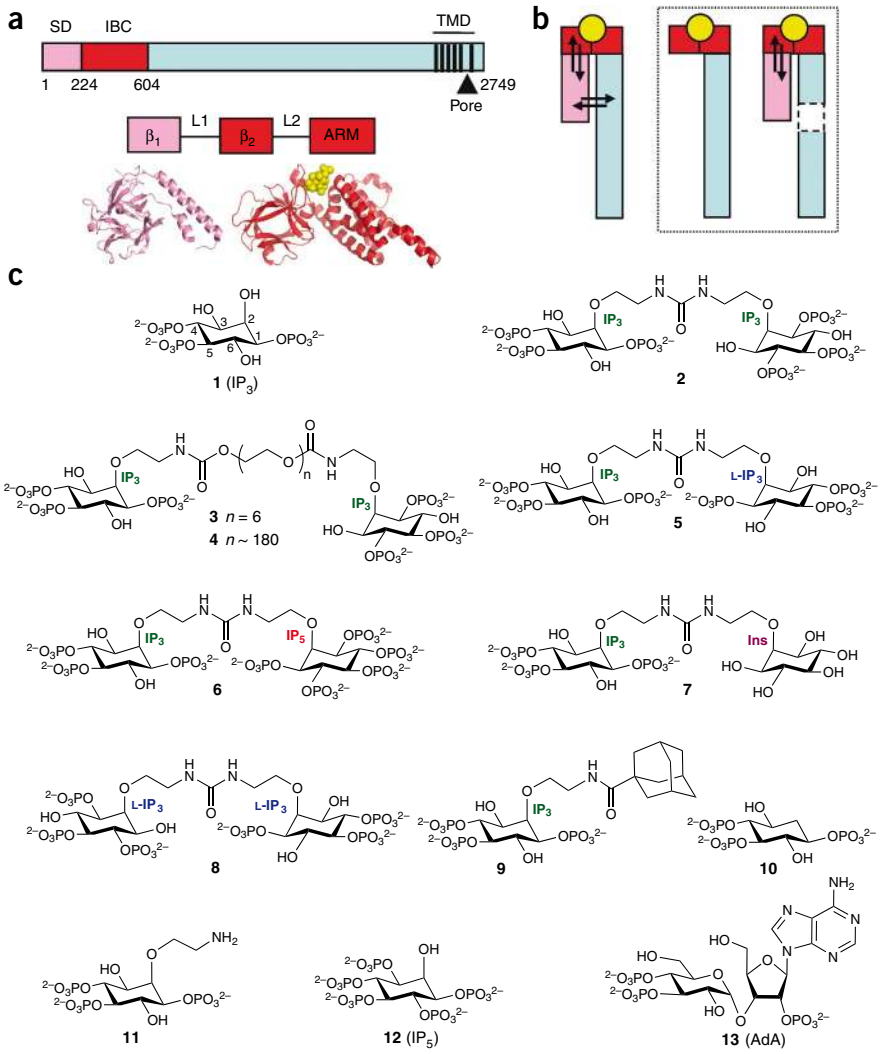

Figure 1 Structure of the IP_3R and its ligands. (**a**) Key domains of IP_3R (numbering from rat IP_3R1, GenBank accession number GQ233032). Pink denotes the SD (residues 1–223), red denotes the IBC (224–604) and black vertical lines represent TMDs. The SD (β_1) and IBC (β_2 and armadillo-like repeat, ARM) comprise three stably folded domains connected by flexible linkers (L1 and L2)[34]. Crystal structures are shown below[3,33]. (**b**) Agonist binding (yellow) to a discrete site on the receptor (IBC for IP_3R, red) evokes conformational changes that propagate through the receptor and that then affect (arrows) the binding site. Removal (boxed diagrams) of a domain through which conformational changes must pass prevents this energetic interplay between conformational changes and binding. (**c**) Structures of the ligands used.

the conformational changes that cause channel opening[10,16,17]. This "binding-gating problem" is a fundamental issue in pharmacology[10], but it can also be turned to advantage because the interplay depends on both the efficacy of the ligand and the presence of the parts of the receptor through which conformational changes must pass. The former is important because partial agonists divert less binding energy than full agonists into effective conformational changes, and the latter is important because receptors lacking essential domains are expected to be less able to divert binding energy into conformational changes (**Fig. 1b**). Analyses of the free energy changes for ligand binding ($\Delta G = RT\ln K_d$, where K_d is the equilibrium dissociation constant) can thus provide insight into the conformational changes evoked by agonist binding. Comparisons of ΔG for full and partial agonists, and for agonist binding to normal and truncated IP_3R, can therefore contribute to defining the links between IP_3 binding and opening of the pore.

Here we synthesize a new series of partial agonists of the IP_3R, and, in defining their properties, we identify a new form of partial agonism that allows us to define key steps in IP_3R activation.

RESULTS

Synthesis of 2-O–modified analogs of IP_3

All high-affinity agonists of all IP_3Rs have structures equivalent to the vicinal 4,5-bisphosphate and 6-hydroxyl of IP_3 (**Fig. 1c**), but the axial 2-hydroxyl is not required[18]. The essential phosphate moieties interact predominantly with opposite sides of the clam-like IBC (P-4 with the β_2 domain and P-5 with the ARM domain)[3] (**Fig. 1a**), which suggests that agonists might close the clam in a manner reminiscent of glutamate binding to iGluR[6,13].

In seeking to develop new high-affinity ligands of IP_3R that might differ in efficacy, we focused on the 2-OH group of IP_3 because earlier structure-activity analyses had suggested that analogs modified at this position retain activity[18]. The X-ray structure of the IBC with IP_3 bound subsequently confirmed that the 2-OH group of IP_3 makes no significant contacts with the IBC[3].

We began by preparing homodimers of IP_3 with linkers of various lengths (**2**, **3** and **4** in **Fig. 1c**), aiming initially to define the separation of IP_3 binding sites within a tetrameric IP_3R. However, informed by our initial results[19,20] and cognizant that dimeric cGMP is a partial agonist of a cGMP-gated cation channel[21], we extended our work to include syntheses of additional 2-O–modified analogs (**Fig. 1c**) and an assessment of their efficacy.

The shortest IP_3 dimer (**2**) is a symmetrically substituted *N*,*N*′-diethylurea synthesized by cross-linking of a protected D-2-*O*-(2-aminoethyl)-IP_3 building block using bis(4-nitrophenyl) carbonate[19]. A modification of this synthetic method was used to synthesize heterodimers such as **5**, **6** and **7**, in which the second IP_3 moiety is replaced by a different inositol phosphate or by inositol (**Scheme 1**). We also synthesized an L-IP_3 homodimer (**8**, the enantiomer of **2**) (**Scheme 1**) and an IP_3-adamantane conjugate (**9**). The syntheses of 2-deoxy-IP_3 (**10**)[22] and 2-*O*-(2-aminoethyl)-IP_3 (**11**)[23] were reported previously. Details of the synthetic procedures and compound characterizations are provided in the **Supplementary Methods**.

2-O–modified IP_3 analogs are high-affinity agonists

We used a cell line that expresses only recombinant rat IP_3R1 (DT40-IP_3R1 cells)[24] to measure Ca^{2+} release from intracellular stores, and IP_3R1 purified from rat cerebellum to measure IP_3 binding. These analyses show that homodimers of IP_3 linked through the 2-O positions of the inositol rings are high-affinity agonists of IP_3R.

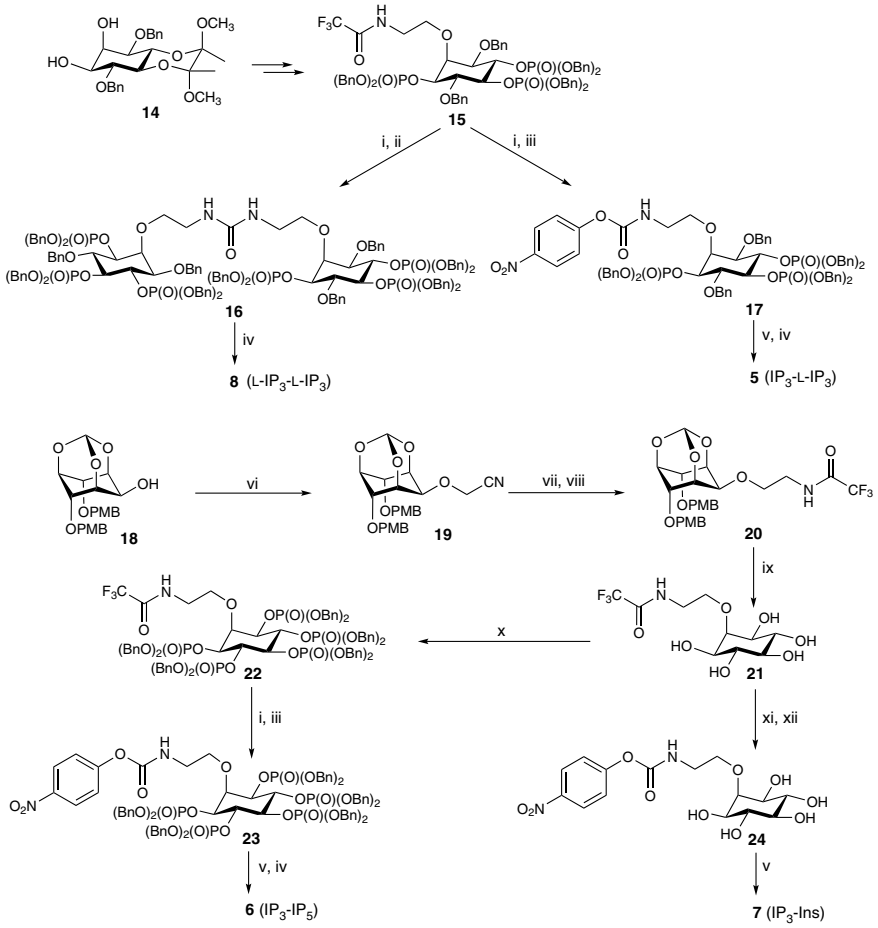

Scheme 1 Syntheses of heterodimers **5**, **6** and **7**, and L-IP_3 dimer **8**. Dimers **5** and **8** were synthesized from L-IP_3–based building block **15**, obtained from diol **14** (ref. 48) (see **Supplementary Methods**). The *N*-trifluoroacetyl protecting group was removed, generating an unstable amine that was reacted with 0.5 equivalents of bis(4-nitrophenyl) carbonate, giving protected L-IP_3 dimer **16**. Hydrogenolytic deprotection of **16** gave L-IP_3 dimer **8**. When 1 equivalent of bis (4-nitrophenyl) carbonate was used, the product was 4-nitrophenyl *N*-alkylcarbamate **17**, which could be isolated and conjugated with D-IP_3 component **11**. The conjugation reaction was carried out in CD_3OD and monitored by ^{31}P NMR spectroscopy. Deprotection followed by anion-exchange chromatography then gave IP_3–L-IP_3 heterodimer **5**. Dimers **6** and **7** were synthesized from alcohol **18** (ref. 49). Nitrile **19** was reduced, and the amine product was temporarily protected as the *N*-trifluoroacetamide (**20**). Acid-labile protecting groups were then removed, giving pentaol **21**, which was converted, via **22**, into carbamate **23**. Carbamate **23** was then conjugated with **11**, and deprotection followed by anion-exchange chromatography gave IP_3–IP_5 heterodimer **6**. Alternatively, conjugation of carbamate **24** with **11** gave IP_3–Ins dimer **7**. Reagents and conditions: (i) LiOH, THF, MeOH, H_2O; (ii) bis (4-nitrophenyl) carbonate (0.5 equiv), THF; (iii) bis(4-nitrophenyl) carbonate (1 equiv), THF; (iv) H_2, $Pd(OH)_2$/C, MeOH, H_2O; (v) **11**, CD_3OD, Et_3N; (vi) NaH, $BrCH_2CN$, CH_3CN; (vii) $LiAlH_4$, THF; (viii) $EtOC(O)CF_3$, THF; (ix) TFA, H_2O; (x) $(BnO)_2PN^iPr_2$, 1*H*-tetrazole, CH_2Cl_2 then 3-chloroperoxybenzoic acid; (xi) Et_3N, H_2O, reflux; (xii) bis(4-nitrophenyl) carbonate (1 equiv), DMF, Et_3N. Bn, benzyl; PMB, 4-methoxybenzyl. DMF, dimethyformamide; TFA, trifluoroacetic acid; THF, tetrahyrofuran. All experimental procedures are described in detail in **Supplementary Methods**.

The shortest dimer (**2**) (**Fig. 1c**) binds to IP_3R1 with greater affinity than IP_3 (**Table 1** and **Supplementary Fig. 1a**) and stimulates Ca^{2+} release from intracellular stores at lower concentrations than does IP_3 (**Table 1** and **Supplementary Fig. 1b**). To our knowledge, **2** is the most potent inositol phosphate–based agonist so far identified.

A homodimer of L-IP_3 (**8**) is, as expected, inactive because L-IP_3 does not bind to the IBC[18]. However, homodimers of IP_3 with longer linkers (**3** and **4**) also bind to IP_3R with greater affinity than IP_3, as do heterodimers in which IP_3 is linked (i) to inositol (inositol-IP_3, **7**), (ii) to an unrelated bulky hydrophobic group (adamantane-IP_3, **9**) or (iii) to an inositol phosphate that does not itself bind to the IBC (IP_3-IP_5, **6**; or IP_3-L-IP_3, **5**) (**Table 1**). The latter (**5**, **6**, **7** and **9**) demonstrate that high-affinity binding of IP_3 dimers does not result from an interaction with a second specific IP_3 binding site, nor does it result from alternating association of the two IP_3 moieties with the IBC[19]. Furthermore, the two components of the dimer must be linked, because a high concentration of IP_5 (**12**, 10 μM) had no effect on the Ca^{2+} release evoked by IP_3 or 2-deoxy-IP_3 (**10**) (**Supplementary Fig. 1c**). We conclude that addition of bulky or charged groups to the 2-O position of IP_3 produces high-affinity agonists of the IP_3R.

A new family of partial agonists of IP_3R

Because a partial agonist activates its receptor less effectively than a full agonist, it must occupy more receptors to evoke the same cellular response[11]. In our Ca^{2+} release assays, where each ligand caused the same maximal Ca^{2+} release as IP_3 (**Table 1**), we can therefore gain some insight into the efficacy of a ligand by comparing the concentration that causes 50% of the maximal response (EC_{50}) with the concentration at which 50% of the binding sites are occupied (K_d).

For each ligand, we compared the EC_{50}/K_d ratio using DT40-IP_3R1 cells for the functional assays[24] (EC_{50}) and purified IP_3R1 to measure IP_3 binding (K_d). Our results suggest that **2** must occupy more IP_3Rs than IP_3 to evoke the same Ca^{2+} release (**2** has a higher EC_{50}/K_d ratio, **Fig. 2a** and **Table 1**). This indicates that **2** may be a partial agonist. These characteristics—an increase in both affinity and EC_{50}/K_d ratio—are shared by very different 2-O–modified IP_3 analogs (**Fig. 2a** and **Table 1**). They do not, therefore, depend on precise structural features: an IP_3 moiety that binds to the IBC and a 2-O substituent larger than adamantane (**9**) are sufficient to increase both the affinity and the EC_{50}/K_d ratio.

The EC_{50}/K_d ratio for adenophostin A (AdA, **13**; **Fig. 1c**)[25], another high-affinity agonist of IP_3R, is similar to that for IP_3 (**Fig. 2a** and **Table 1**). This is consistent with single channel analyses, where IP_3 and AdA cause the IP_3R to open to the same maximal single channel open probability (P_o, the fraction of time that each channel spends in its open state) (**Fig. 2b** and **Supplementary Table 1**)[26]. We conclude that IP_3 and AdA are full agonists of the IP_3R, whereas **2**–**7** and **9** appear to be partial agonists.

Table 1 Responses to IP_3 analogs

		Ca^{2+} release		FL		NT	IBC
		EC_{50} (nM)	Release %	K_d (nM)	EC_{50}/K_d	K_d (nM)	K_d (nM)
1	IP_3	20 ± 2	77 ± 5	12.5 ± 1.06	1.6 ± 0.2	2.82 ± 0.26	0.21 ± 0.03
13	AdA	1.5 ± 0.1	75 ± 6	1.26 ± 0.11	1.2 ± 0.01	ND	ND
2	$(IP_3)_2$ 0.8 nm	2.7 ± 0.4	76 ± 6	0.45 ± 0.04	6.0 ± 1.0	0.41 ± 0.03	0.18 ± 0.01
3	$(IP_3)_2$ 1.5 nm	4.9 ± 0.3	74 ± 6	0.86 ± 0.19	5.7 ± 1.3	0.47 ± 0.09	0.18 ± 0.01
4	$(IP_3)_2$ 8 nm	13 ± 1	73 ± 7	1.39 ± 0.23	9.3 ± 1.6	1.37 ± 0.20	0.48 ± 0.02
5	IP_3–L-IP_3 0.8 nm	5 ± 1	70 ± 7	0.90 ± 0.12	5.6 ± 1.3	0.42 ± 0.02	0.14 ± 0.02
6	IP_3–IP_5 0.8 nm	5 ± 0	72 ± 5	0.89 ± 0.11	5.6 ± 0.7	0.36 ± 0.03	0.20 ± 0.01
7	IP_3–Ins 0.8 nm	21 ± 1	76 ± 4	7.82 ± 1.73	2.7 ± 0.6	2.81 ± 0.22	0.33 ± 0.01
8	(L-IP_3)$_2$ 0.8 nm	Inactive*	ND	ND	ND	ND	ND
9	2-adamantane-IP_3	30 ± 3	71 ± 1	7.62 ± 0.51	3.9 ± 0.5	1.63 ± 0.02	0.20 ± 0.02
10	2-deoxy-IP_3	32 ± 7	65 ± 3	17.1 ± 1.1	1.9 ± 0.4	4.01 ± 0.38	0.22 ± 0.03
11	2-aminoethyl-IP_3	42 ± 5	69 ± 6	43.6 ± 4.6	0.95 ± 0.02	13.5 ± 2.0	0.52 ± 0.04

The effects of each analog on Ca^{2+} release from the intracellular stores of permeabilized DT40-IP_3R1 cells and on ^{3}H-IP_3 binding to full-length purified IP_3R1 (FL), its N terminus (NT, residues 1–604) or the IBC (residues 224–604) are summarized (n ≥ 4). For dimers, the estimated separation of the two moieties is shown (calculated as in ref. 50). Results are means ± s.e.m.
*No detectable Ca^{2+} release with 30 μM **8**. ND, not determined.

envelope of DT40-IP_3R1 cells to resolve the behavior of single IP_3R. To maximize the amplitude of the currents recorded and to avoid the complexity of feedback regulation of IP_3R by Ca^{2+} passing through them[1], we used K^+ as the charge carrier in these experiments[26,27]. Both the single channel K^+ conductance (γ_K) and the mean channel open time (τ_o) were the same for all agonists examined (**Fig. 2b,d** and **Supplementary Table 1**). The open state of the IP_3R thus appears to be similar whether it is evoked by binding of a full agonist (AdA, IP_3 and **10**) or a partial agonist (**2**, **6** and **9**).

However, for IP_3R activated by maximal concentrations of AdA, IP_3 or **10**, P_o was higher than with **2**, **6** or **9** (**Fig. 2b,e** and **Supplementary Table 1**). Increasing the concentration of **2** (from 0.5 to 10 μM, **Fig. 2b,e**) did not further increase P_o, and after stimulation with a mixture of IP_3 and **2** (10 μM of each), P_o was significantly ($P < 0.05$) lower than with IP_3 alone (**Fig. 2b** and **Supplementary Table 1**). These analyses of single IP_3Rs confirm and extend the results obtained with the Ca^{2+} release and binding assays (**Table 1** and **Fig. 2a**). Analogs of IP_3 with bulky additions to the 2-O position (**2**–**7** and **9**) are high-affinity partial agonists of IP_3R1. Subsequent analyses of the mechanisms underlying these properties of the 2-O–substituted analogs focus on **2** (**Fig. 1c**).

The results shown in **Figure 2c** confirm that **2** must occupy more IP_3Rs than the full agonist, AdA, to evoke the same Ca^{2+} release. DT40-IP_3R1 cells were first pretreated with concentrations of AdA or **2** that caused the same Ca^{2+} release (5.7 ± 1.0% and 5.4 ± 1.3% of the intracellular Ca^{2+} stores, respectively) and then stimulated with IP_3. More IP_3 was required to evoke further Ca^{2+} release after treatment with **2** than after treatment with AdA (EC_{50} = 44.4 ± 3.19 and 4.37 ± 0.18 nM, respectively). This confirms that **2** must occupy more IP_3R than AdA to evoke the same Ca^{2+} release.

Because the nuclear envelope is continuous with the endoplasmic reticulum[26], we can use patch-clamp recording from the outer nuclear

Our single channel analysis shows that whereas τ_o is similar for all agonists (**Supplementary Table 1**), mean channel closed times (τ_c) were longer for the partial agonists (**2**, **6** and **9**) than for full agonists (IP_3, AdA and **10**) (**Fig. 2e** and **Supplementary Table 1**). The latter, assuming a very simplified activation scheme (**Fig. 2e** and **Supplementary Methods**), reveals that the rate constant for channel

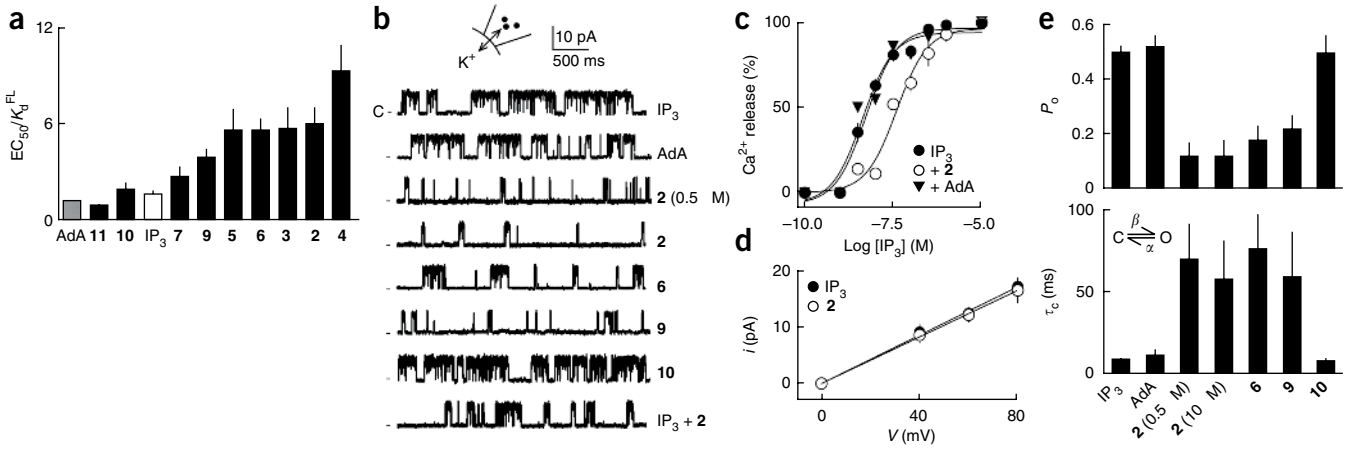

Figure 2 2-O–modified IP_3 analogs are partial agonists of IP_3R. (**a**) From experiments similar to those shown in **Supplementary Figure 1a,b**, EC_{50}/K_d ratios ($n \geq 4$) were calculated for each ligand. FL, full-length purified IP_3R1. (**b**) Traces (each typical of at least three similar records) show excised nuclear patch-clamp recordings from DT40-IP_3R1 cells with the pipette solution containing ATP (0.5 mM), a free [Ca^{2+}] of 200 nM and the indicated ligands (10 μM, except where shown otherwise). The holding potential was +40 mV. C denotes the closed state. (**c**) Cells were treated with IP_3 alone, or for 30 s with 0.1 nM AdA or 0.1 nM **2** and then with the indicated concentrations of IP_3. Results ($n = 3$) show the concentration-dependent release of Ca^{2+} by IP_3. (**d**) Current-voltage (*i-V*) relationship for patches stimulated with IP_3 or **2** (means ± s.e.m., $n = 3$). (**e**) Summary data showing P_o and mean closed time (τ_c) for IP_3R1 stimulated as shown, $n = 3$–11 (further details in **Supplementary Table 1**). The simplified activation scheme for IP_3R shows the transition between closed (C) and open (O) states determined by rate constants β and α (see **Supplementary Methods**). All results (**a**,**c**–**e**) are means ± s.e.m.

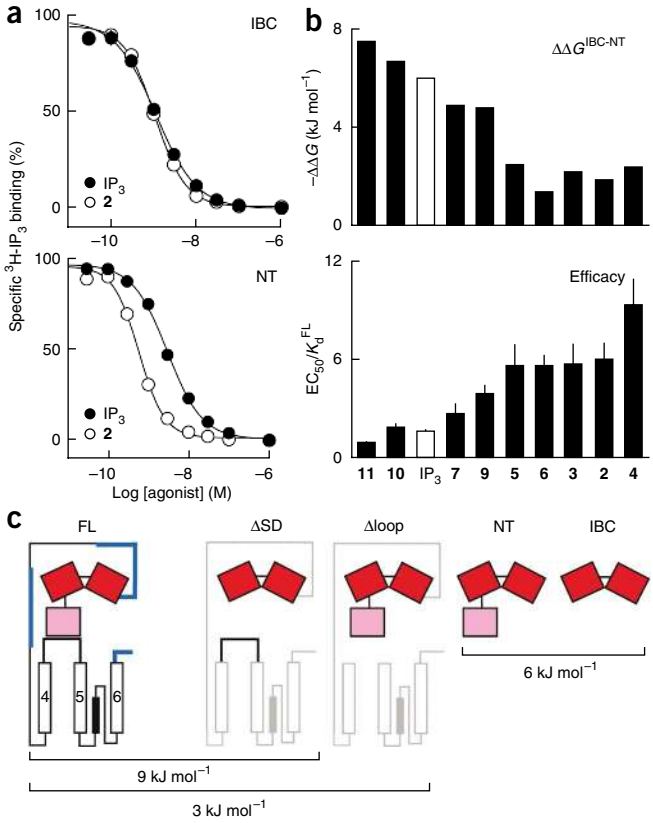

Figure 3 Partial agonists are similar to IP_3 in their interactions with the IBC. (**a**) Equilibrium competition binding to isolated IBC (top) and NT (bottom) with ^{3}H-IP_3 and either IP_3 or **2**, $n \geq 17$. (**b**) $\Delta\Delta G$ ($\Delta G^{IBC} - \Delta G^{NT}$), which reflects ΔG used to rearrange the IBC-SD relationship, is shown for each ligand and compared with the efficacy of each (EC_{50}/K_d, with K_d determined for full-length IP_3R1). Results (**a**,**b**) are means ± s.e.m. (**c**) Estimated ΔG for conformational changes associated with IP_3R activation. The affinity (K_d) of IP_3 for IP_3R1 truncated as shown was measured herein (**Table 1**) or by others, for ΔSD (ref. 4; IP_3R1 lacking residues 1–223) and for Δloop (ref. 32; IP_3R1 lacking residues 2428–2437); ΔG was then calculated from $\Delta G = RT\ln K_d$. The K_d for IP_3 was not directly measured in ref. 32, but under the conditions used the fourfold increase in IP_3 binding after deletion of residues 2428–2437 (that is, Δloop) is likely to reflect a fourfold decrease in K_d. We assume that deletion of IP_3R fragments through which conformational changes must pass increases IP_3 affinity because less binding energy is diverted into rearranging the protein (**Fig. 1b**). Deletions of many other regions (shown in blue) do not increase IP_3 affinity[4], which suggests that the IP_3-evoked conformational changes do not pass through them. This analysis is consistent with each IP_3 binding event diverting ~9 kJ mol^{-1} into conformational changes of the IP_3R, of which ~6 kJ mol^{-1} rearranges the SD-IBC relationship and ~3 kJ mol^{-1} is used by the SD to gate the pore.

opening ($\beta = 1/\tau_c$) with partial agonists is less than with full agonists. The 2-O–modified analogs are the first partial agonists of IP_3R for which the basis of their reduced efficacy has been established. They open the channel fully (**Fig. 2b**,**d**) and the channel closes at the same rate whether it has a partial agonist or IP_3 bound (α in **Fig. 2e**), but the rate constant for channel opening (β) is lower for partial agonists (**Fig. 2e** and **Supplementary Table 1**). We conclude that these full and partial agonists drive the IP_3R into a similar open state, but the partial agonists do so less effectively. A similar situation holds for glycine and nicotinic acetylcholine receptors[7].

Partial agonists differ in how they rearrange the IBC-SD

For IP_3R, conformational changes evoked by IP_3 binding to the IBC near the N terminus must be transmitted to the pore formed by residues close to the C terminus (**Fig. 1a**). Some of the energy provided by IP_3 binding is used to drive the opening of the pore. The K_d ($\Delta G = RT\ln K_d$) measured in a binding assay is therefore determined by both the strength of the contacts between IP_3 and the IBC ("intrinsic binding affinity")[16] and the ensuing conformational changes[10]. Because IP_3 binds independently to each subunit of a tetrameric IP_3R (**Supplementary Fig. 1a**), our subsequent studies of IP_3R activation combine analyses of tetrameric IP_3R with measurements of IP_3 binding to monomeric N-terminal fragments.

The IBC includes all the amino acid residues that contact IP_3 (**Fig. 1a**)[3,28], and each 2-O–modified agonist (**2**–**7** and **9**–**11**) (**Fig. 1c**) retains the groups within IP_3 that interact with the IBC. Furthermore, each of these ligands binds with similar affinity to the IBC alone (**Fig. 3a** and **Table 1**). Because the full (IP_3) and partial agonists (**2**–**7** and **9**) are both expected to make the same contacts with the IBC and are also observed to bind to it with similar affinity, we suggest that they do not differ in the binding energy they divert into changing the conformation of the IBC. This contrasts with AMPA receptors, where the clam-like binding site closes more fully with more efficacious agonists[12,13]. The distinction highlights two fundamentally different ways of reducing efficacy, a defining feature of all ligand-receptor interactions[10]. A partial agonist may fail to make optimal contacts with the binding site and thereby less effectively activate the receptor (for example, AMPA receptors[12]), or it may impair onward transmission of conformational changes. Subsequent experiments demonstrate that our partial agonists (**2**–**7** and **9**) belong to the second category. They are therefore useful in defining the steps that follow IP_3 binding.

For all three IP_3R subtypes, IP_3 binds to the isolated IBC with greater affinity than to either full-length IP_3R or the isolated N terminus (NT, residues 1–604) (**Fig. 3a**, **Table 1** and **Supplementary Table 2**)[28,29]. The SD reduces the IP_3 binding affinity through its intramolecular interaction with the IBC[28] and also appears to mediate communication between the IBC and the pore[4,5]. We therefore examined the contribution of the SD to the conformational changes initiated by IP_3 via analysis of ΔG for ligand binding.

Removal of the SD from the isolated NT (to produce the IBC fragment) increases its affinity for IP_3, but it has lesser effects on binding of the partial agonists (**Table 1**). Efficacy (reported by the EC_{50}/K_d ratio) and the difference in ΔG ($\Delta G = RT\ln K_d$) for binding to the isolated IBC and NT ($\Delta\Delta G$) are inversely correlated (**Fig. 3b**). Because we suggest that each agonist contributes similar intrinsic binding energy[16,17] through the similar interactions that each makes with the IBC (**Table 1** and **Supplementary Table 2**), the different $\Delta\Delta G$ for binding of full and partial agonists to the NT must reflect the extent to which each uses binding energy to rearrange the relationship between the IBC and SD[16,17,30]. We conclude that full and partial agonists differ minimally in their interactions with the IBC, but they differ radically in how they rearrange its relationship with the SD.

Conformational changes are transmitted entirely via the SD

IP_3 binds only to a small contiguous sequence within the IP_3R: the IBC (**Fig. 1a**). Truncations of the IP_3R might therefore disconnect IP_3 binding from downstream conformational changes without directly perturbing the IP_3 binding site. These truncated IP_3Rs might then reveal, via analysis of ΔG for ligand binding, the parts of the IP_3R through which IP_3-evoked conformational changes must pass (**Fig. 1b**).

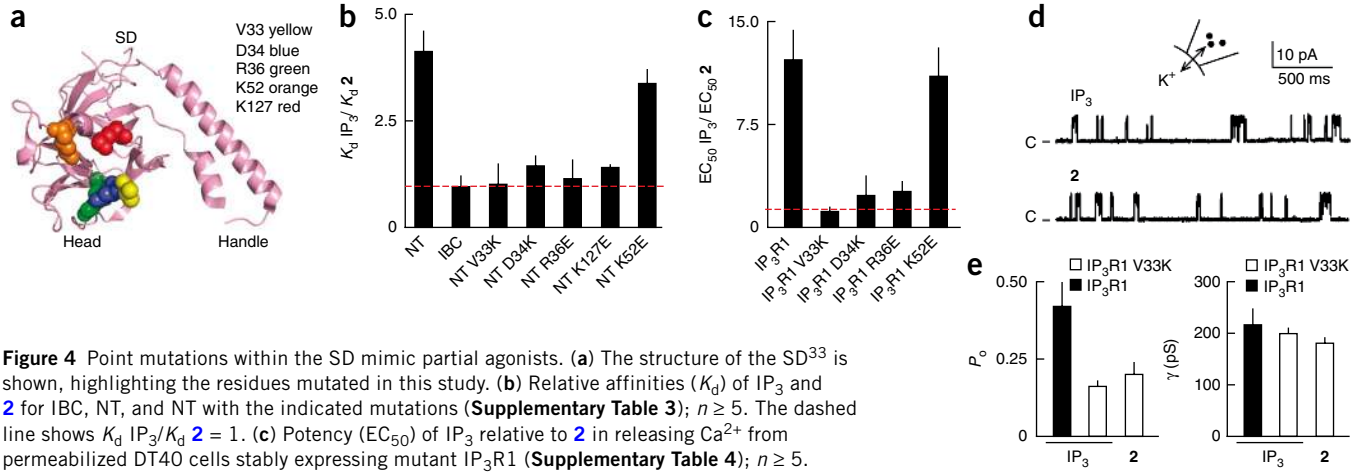

Figure 4 Point mutations within the SD mimic partial agonists. (**a**) The structure of the SD[33] is shown, highlighting the residues mutated in this study. (**b**) Relative affinities (K_d) of IP_3 and **2** for IBC, NT, and NT with the indicated mutations (**Supplementary Table 3**); $n \geq 5$. The dashed line shows K_d IP_3/K_d **2** = 1. (**c**) Potency (EC_{50}) of IP_3 relative to **2** in releasing Ca^{2+} from permeabilized DT40 cells stably expressing mutant IP_3R1 (**Supplementary Table 4**); $n \geq 5$. The dashed line shows EC_{50} IP_3/EC_{50} **2** = 1. (**d**) Typical recordings from excised nuclear patches of DT40-IP_3R1 V33K cells with 10 μM IP_3 or **2** in the patch pipette. The holding potential was +40 mV. C denotes the closed state. (**e**) Summary data showing P_o and γ_K for IP_3R1 and IP_3R1 V33K stimulated with 10 μM IP_3 or **2**; $n \geq 3$. Results (**b**,**c**,**e**) are means ± s.e.m.

All full-length IP_3R subtypes bind IP_3 with only slightly lower affinity than the isolated NT ($\Delta\Delta G \sim 3$ kJ mol^{-1})[28], whereas the NT and IBC differ more substantially in their affinities for IP_3 (~6 kJ mol^{-1}) (**Table 1** and **Supplementary Table 2**). This suggests that the most costly conformational changes evoked by IP_3 occur within the NT (~6 kJ mol^{-1}), with downstream events requiring less energy (~3 kJ mol^{-1}) (**Fig. 3c**). Removing the SD from full-length IP_3R increases its affinity for IP_3 by an amount (≤ about −9 kJ mol^{-1})[4] that is consistent with uncoupling IP_3 binding from all the conformational changes downstream of the IBC (**Fig. 3c**). These analyses suggest that the IBC communicates with the rest of the IP_3R entirely via the SD.

A site within the first 340 residues of the IP_3R, which includes the SD, appears to interact with a short cytosolic loop linking TMD4 and TMD5 (**Fig. 3c**). This interaction has been proposed to open the pore directly[31,32]. Disruption of this loop within a full-length IP_3R increases its affinity for IP_3 by an amount (about −3 kJ mol^{-1})[32] that matches the estimated cost of all conformational changes downstream of the SD (**Fig. 3c**).

These analyses corroborate our suggestion that conformational changes pass directly and exclusively from the IBC to the SD, and then perhaps directly to the TMD4-TMD5 loop[31,32].

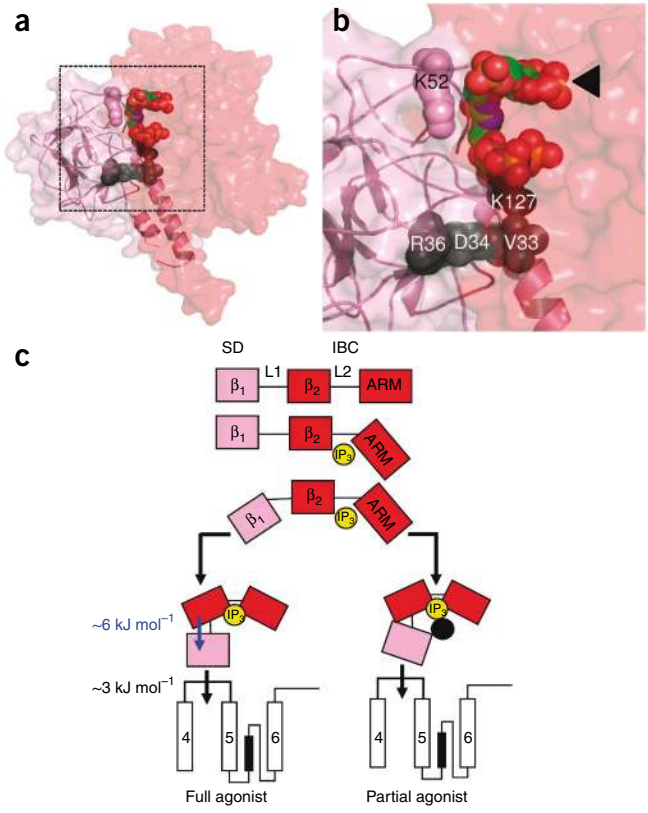

Figure 5 IP_3 binding to the IBC activates IP_3R entirely via the SD. (**a**,**b**) Predicted relationship between the SD (pink) and IBC (red) with **2** bound. Residues within the SD that affect efficacy (Val33, Asp34, Arg36 and Lys127) are shown in black (see **Fig. 4a** and **Supplementary Fig. 3** for details). The ineffective residue Lys52 is shown in pink. **b** is an enlargement of the boxed area in **a**, with the IBC-bound IP_3 moiety indicated by an arrow. (**c**) IP_3 (yellow) rearranges the two domains of the IBC (β_2 and ARM, red) around its L2 loop, causing rearrangement of the SD (β_1, pink) around the L1 loop. The SD is then entirely responsible for transmitting conformational changes toward the pore, probably by directly interacting with the TMD4-TMD5 loop of an adjacent subunit[31,32]. ΔG associated with rearranging the SD and its subsequent communication with the pore region is shown. Partial agonists effectively rearrange the IBC, but the inositol 2-O substituent (or point mutations in the SD; black circle) disrupts the IBC-SD interface and thus blocks communication with the SD. The latter is now less likely to contact the TMD4-TMD5 loop, but once it makes contact, the channel gates normally.

Point mutations within the SD mimic partial agonists

Removal of the SD and additions to the 2-O position of IP_3 similarly increase binding affinity (**Table 1**). We suggest that the latter occurs because the analogs evoke lesser conformational changes in the IP_3R. Both modifications also uncouple ligand binding from gating, although removal of the SD does so more completely[4,5] than do the 2-O modifications to IP_3. We therefore speculated that 2-O–modified analogs partially mimic removal of the SD by disrupting its interaction with the IBC and that this causes both a decrease in efficacy and an increase in affinity.

The SD has a structure reminiscent of a hammer with a large head and a short handle (described earlier as an "arm")[33] (**Fig. 4a**). Others[33] have shown that removing the handle of the SD (residues 67–108) minimally affects IP_3 binding to the NT. But mutation of highly conserved residues on the surface of the head domain, most notably within the β2-β3 loop (loop 2)[33], increases the affinity of the NT for

IP_3. We therefore tested our hypothesis that 2-O–modified analogs of IP_3 disrupt the IBC-SD interface by mutagenesis of residues in the β2-β3 loop and of other residues nearby in the three-dimensional structure of the SD (**Fig. 4a**). As reported[33], several mutations increased the affinity of the NT for IP_3, with the most effective (V33K) almost mimicking the effect of removing the entire SD. Another mutation (K52E) had no effect (**Supplementary Table 3**)[33]. Furthermore, and consistent with our suggestion that 2-O substituents of IP_3 disrupt the IBC-SD interaction, the effective mutations had less pronounced effects on binding of **2** to the NT (**Fig. 4b** and **Supplementary Table 3**). From these non-additive effects, we conclude that binding of **2** displaces the SD in a manner that mimics its removal or displacement by appropriate mutations.

Our results so far establish that the 2-O substituents of the IP_3 analogs and appropriate point mutations within the SD cause similar increases in binding affinity. These effects mimic removal of the SD, leading us to conclude that they result from disrupted communication between the IBC and SD. Given that the 2-O–substituted analogs are partial agonists, and that the SD is required for IP_3 to gate the pore[4,5], we speculated that the point mutations might further mimic the analogs and produce IP_3Rs that even full agonists are unable to activate fully.

In DT40 cells expressing IP_3R1 mutated within the SD (**Fig. 4a** and **Supplementary Fig. 2a**,**b**), IP_3 and **2** evoke Ca^{2+} release from permeabilized cells and activate IP_3R in nuclear patch-clamp recordings (**Fig. 4c–e**, **Supplementary Fig. 2c** and **Supplementary Table 4**). The properties of these interactions are consistent with our prediction that disrupting the IBC-SD interaction decreases efficacy and increases agonist affinity by blocking propagation of conformational changes from the IBC. In permeabilized DT40 cells expressing IP_3R1 with the V33K mutation (IP_3R1 V33K), IP_3 and **2** are equipotent (**Supplementary Fig. 2c**), and in single channel recordings they have the same P_o (**Fig. 4d**,**e**). This P_o is similar to that observed for normal IP_3R stimulated with **2**, but lower than the P_o with IP_3 (**Fig. 2b**,**e**). The less effective mutations have less pronounced effects (**Fig. 4c**), which is consistent with our suggestion that they cause lesser disruption of the IBC-SD interaction.

The structures of the IBC-IP_3 and SD are known[3,33] (**Fig. 1a**), but the relationship between them is not known[34]. We used protein-protein docking to identify a likely relationship between them (**Supplementary Methods**). The three IP_3R subtypes differ in their affinities for IP_3, but their IBCs share similar sequences and bind IP_3 with the same affinity[28]. A subtype-specific interaction between the IBC and SD determines the different affinities of the three full-length IP_3Rs[28]. Because the residues within the SD that confer these subtype-selective interactions[28,33] are likely to lie at an IBC-SD interface, this criterion was used to select between possible models of the IBC-SD complex. Our proposed model (**Fig. 5a**,**b** and **Supplementary Fig. 3**) is consistent with the radius of the NT-IP_3 complex obtained from small-angle X-ray scattering[34]. In this structure, four of the loops (loops 2 and 5, and part of loops 3 and 7)[33] that link the β-strands of the SD interact primarily with loops from the β_2-domain of the IBC (**Supplementary Fig. 3**). Within this IBC-SD structure, the second IP_3 moiety of **2** lies close to several point mutations in the SD (V33K, D34R and R36E) that reduce efficacy (**Supplementary Table 4**), each lying on the putative IBC-SD interface (within loop 2). The same interface includes the other effective mutation (K127E, within loop 5) but not the ineffective one (K52E) (**Fig. 5a**,**b** and **Supplementary Fig. 3c**,**d**).

We conclude that bulky or charged groups introduced into the IBC-SD interface by either the ligand or the SD disrupt essential communication between the IBC and SD and thereby reduce efficacy.

DISCUSSION

We have synthesized and characterized a family of partial agonists of IP_3R that differ minimally from full agonists in their interactions with the binding site (IBC), but that have reduced efficacy because they block an obligatory communication between the IBC and SD. These results define two fundamentally different routes to reduced efficacy. A partial agonist may fail to make optimal contacts with the ligand binding site[12,13,35]. Alternatively, it may (as we have shown for our partial agonists of IP_3R) bind normally and then through additional interactions block onward transmission of essential conformational changes. These new properties of our partial agonists allow us to show that the conformational changes initiated at the IBC pass entirely via the SD to the pore (**Fig. 5c**).

Our activation scheme is consistent with an earlier proposal that IP_3 minimally affects the structures of the three domains of the NT, but rearranges their relationships via flexible linking loops[34] (**Fig. 5c**). We suggest that IP_3 first stabilizes interaction of the β_2 and ARM domains of the IBC by interacting with residues in each[3,36]. These interactions require the 4- and 5-phosphate groups of IP_3. The IBC then interacts with the SD (β_1 in **Fig. 5c**) to give a compact structure[34] that allows the SD alone to signal onwards to the pore, probably via its interaction with the TMD4-TMD5 loop (**Fig. 5c**)[32].

IP_3Rs are close relatives of ryanodine receptors (RyR); they share most of their sequence similarity within their N termini and pores. The likely structural similarities between the SD of IP_3R and the N terminus of RyR suggest that these regions may have similar functions in both families of intracellular Ca^{2+} channels[33]. Mutations that cause RyR to become dysfunctional in malignant hyperthermia, central core disease (RyR1) and catecholaminergic polymorphic ventricular tachycardia (RyR2) cluster in four regions that include the N terminus and a region close to the pore[37]. Furthermore, three-dimensional reconstructions of RyR have shown that activation is associated with major conformational changes within a region that includes the N terminus[38]. For RyR1, the same region includes residues that interact with the dihydropyridine receptor, which is the major physiological regulator of RyR1. From structure-based sequence alignment[36], it has been suggested that the SD surface opposite to that which we suggest contacts the IBC (**Supplementary Fig. 3e**,**f**) is most conserved between IP_3R and RyR. We speculate that this may be the surface that communicates with the conserved pore region for both IP_3R and RyR.

The SD of an IP_3R activated by a partial agonist fully engages the structures that open the pore because an open IP_3R is the same whether activated by a full or partial agonist (**Fig. 2b**,**d** and **Supplementary Table 1**), but it does so less frequently than when activated by a full agonist (**Fig. 5c**). The many additional proteins that interact with the SD[1,33] may exert their effects on IP_3R by targeting this essential link between IP_3 binding and channel opening.

In conclusion, we have synthesized a family of 2-O–modified analogs of IP_3 and shown that they are partial agonists of IP_3R. IP_3 and these partial agonists interact similarly with the IBC, but the 2-O substituents of the analogs block transmission of essential conformational changes from the IBC to the SD. The partial agonists thereby open the channel less effectively. This unusual form of partial agonism allows us to define two means whereby a ligand may have reduced efficacy: either it may fail to make optimal contacts with the binding site, or it may bind like a full agonist but then interfere with subsequent conformational changes. By combining mutagenesis of IP_3R with analyses of the effects of these new partial agonists, we have shown that the major conformational changes evoked by IP_3 occur within the N terminus and pass to the pore entirely via the SD (**Fig. 5c**).

METHODS

Synthesis of ligands. Adenophostin A (**13**)[39], inositol 1,3,4,5,6-pentakisphosphate (IP_5, **12**)[40], IP_3 dimers[19] **2**, **3** and **4**, D-2-deoxy-IP_3 (**10**)[22] and 2-*O*-(2-aminoethyl)-IP_3 (**11**)[23] were synthesized as previously reported. Details of the syntheses of compounds **5**–**9** are given in **Supplementary Methods**. IP_3 was from Alexis. ^{3}H-IP_3 (18–23 Ci mmol^{-1}) was from PerkinElmer.

Stable expression of IP_3R1 in DT40 cells. Rat IP_3R1s (GenBank accession number GQ233032) were stably expressed in DT40 cells in which the genes for all endogenous IP_3R had been disrupted[41]. The open reading frame[42] of rat IP_3R1 without its S1 splice site (S1$^-$) was amplified by PCR using primers P6 and P7 and cloned as an EcoRI fragment into pcDNA3. The CMV (cytomegalovirus) promoter was replaced by the chicken β-actin hybrid promoter, which was excised from the vector pAneo[41], to produce the construct pcDNA3-IP_3R1. A QuikChange II XL site-directed mutagenesis kit (Stratagene) was used to introduce point mutations in rat IP_3R1, which had been previously cloned into the pENTR1A vector. The primers are listed in **Supplementary Table 5**. Mutated IP_3R1 was subcloned into pcDNA3.2 by recombination (Gateway, Invitrogen). The sequences of all full-length IP_3R constructs were confirmed. DT40 cells stably expressing IP_3R1 and its mutants were generated and cultured as described[24]. Expression of mutant IP_3R in DT40 cell lines was quantified by immunoblotting (**Supplementary Fig. 2a**,**b**).

Functional assay of IP_3R1 in DT40 cells. A low-affinity Ca^{2+} indicator (Mag-fluo-4) trapped within the intracellular Ca^{2+} stores was used to measure IP_3-evoked Ca^{2+} release[24].

Cloning and mutagenesis of N-terminal fragments of IP_3R1. Appropriate regions of rat IP_3R1 were amplified by PCR from the full-length receptor clone lacking the S1 splice region (S1$^-$). Fragments are numbered by reference to the full-length (S1$^+$) rat IP_3R1. PCR used P1 and P2 primers for the fragment including residues 1–604 (NT), and P3 and P2 for residues 224–604 (IBC). Both P1 and P3 insert a thrombin-cleavage site. Fragments were ligated into the pTrcHisA vector at the XhoI and EcoRI sites (Invitrogen) to allow expression of N-terminally tagged His_6 proteins. For insertion of the S1 splice region into the IBC fragment, we used a QuikChange mutagenesis kit with P4 and P5 primers. For mutagenesis of residues within the SD, we used the same kit. The primers are listed in **Supplementary Tables 5** and **6**. The sequences of all constructs were confirmed by DNA sequencing.

Expression of IP_3R1 fragments in bacteria. Constructs were transformed into *Escherichia coli* BL21(DE3)[43], and 1 ml of the culture was grown overnight at 37 °C in Luria-Bertani medium (LBM) with 50 μg ml^{-1} ampicillin. The inoculum was cultured at 22 °C in 100 ml of LBM until the optical density at 600 nm (OD_{600}) reached 1.0–1.5. Next, isopropyl β-D-thiogalactoside (0.5 mM) was added, and after 20 h at 15 °C, cells were harvested (5,000*g*, 5 min). The pellet was resuspended in Tris/EDTA medium (TEM: 50 mM Tris, 1 mM EDTA, pH 8.3) supplemented with 10% (v/v) Pop-Culture (Novagen), 1 mM 2-mercaptoethanol and protease inhibitor cocktail (Sigma). The suspension was incubated with lysozyme (100 μg ml^{-1}) and RNase (10 μg ml^{-1}) for 30 min on ice, and the lysate was sonicated for 20 s. After centrifugation (30,000*g*, 60 min), aliquots of supernatant were frozen in liquid nitrogen and stored at −80 °C.

For immunoblotting, samples were loaded onto SDS-PAGE gels and transferred to Immobilon membranes (Millipore), and His_6-tagged proteins were identified using an anti-His_6 antibody. Proteins were cleaved from their His_6 tags by incubating bacterial lysates with biotinylated thrombin (Novagen), and thrombin was removed with streptavidin-agarose (Novagen). Cleavage was monitored by immunoblotting using anti-His_6 and Ab1 (ref. 42) or Ab1.1 antisera for the NT and IBC fragments, respectively (**Supplementary Fig. 4** and **Supplementary Methods**).

Purification of IP_3R1 from rat cerebellum. IP_3R1 was purified at 4 °C from cerebella of adult rats using heparin-affinity chromatography[44]. Frozen cerebella were homogenized in homogenization medium (1 M NaCl, 1 mM EDTA, 50 mM Tris, 1 mM benzamidine, protease inhibitor cocktail tablet (Roche), pH 8.3) and centrifuged (100,000*g*, 30 min). The pellet was solubilized in homogenization medium without NaCl and supplemented with 1.2% (w/v) CHAPS. After centrifugation (100,000*g*, 1 h), the NaCl concentration of the supernatant was increased to 250 mM before loading onto heparin-agarose beads (Sigma). After 30 min, the beads were washed twice in glycerol-containing medium (250 mM NaCl, 50 mM Tris, 10% (v/v) glycerol, 1 mM 2-mercaptoethanol, 1 mM benzamidine, 1 mM EGTA, 1% (w/v) CHAPS, Roche protease inhibitor cocktail, pH 8.0). IP_3Rs were then eluted with elution medium (500 mM NaCl, 50 mM Tris, 10% (v/v) glycerol, 1 mM 2-mercaptoethanol, 1 mM benzamidine, 1 mM EGTA, 50 mM Tris, 1% (w/v) CHAPS, pH 8.0), and aliquots were frozen in liquid nitrogen before storage at −80 °C.

^{3}H-IP_3 binding. Equilibrium competition binding assays were performed at 4 °C for 5 min in TEM containing ^{3}H-IP_3 (18–23 Ci mmol^{-1}, 0.2–1.5 nM), bacterial lysate (5–10 μg) or purified IP_3R (2.5 μg), and competing ligands. Results were analyzed by fitting to a Hill equation (GraphPad Prism) from which the half-maximal inhibitory concentration (IC_{50}) and thereby the K_d were calculated. The variance of the ratios of mean values (a and b) was calculated from the variances (var) of each[45]: $\mathrm{var}(a/b) = (a/b)^2[(\mathrm{var}(a)/a^2) + (\mathrm{var}(b)/b^2)]$.

Single channel recording. We performed patch-clamp recording from excised nuclear patches of DT40 cells as reported previously[26,27]. IP_3Rs are relatively nonselective cation channels ($P_{Ba}/P_K \sim 6$)[1]. K^+ was therefore used as charge carrier to increase single channel current amplitudes[26] and to avoid feedback regulation of IP_3R by permeating Ca^{2+}. QuB (http://www.qub.buffalo.edu) was used for analysis of all channel records (**Supplementary Methods**).

Molecular modeling. We developed a model of the IBC-SD relationship from the Protein Data Bank coordinate files for the IBC (1N4K) and SD (1XZZ) using protein-protein docking. Coarse-grained models of the complex were first produced using Hex5.1 (http://www.csd.abdn.ac.uk/hex/)[46]. From these models we selected those in which the linked termini of the SD and IBC were appropriately separated, and then considered only those models in which residues from the SD known to affect binding of IP_3 to the IBC[28,33] were located at an IBC-SD interface. A representative structure was further refined using a local docking search with RosettaDock[47]. Detailed methods are given in **Supplementary Methods**. Our predicted structure of the IBC-SD complex (**Fig. 5a**,**b** and **Supplementary Fig. 3**) has an inertial radius of gyration (26.1 Å) that is compatible with the Guinier radius of gyration (30.7 Å) obtained by small-angle X-ray scattering[34].

Accession codes. GenBank: Rat IP_3R1 (GQ233032). Protein Data Bank: IBC (1N4K) and SD (1XZZ).

Note: Supplementary information and chemical compound information is available on the Nature Chemical Biology website.

ACKNOWLEDGMENTS

We thank S. Dedos, P. da Fonseca, A. Burgen, S. Otto and M. Garcia Alai for helpful comments, and T. Woodman for advice on NMR spectroscopy. This work was supported by grants from the Wellcome Trust (to C.W.T., A.M. Riley and B.V.L.P.) and the Biotechnology and Biological Sciences Research Council (to C.W.T.). A.M. Rossi holds a Junior Research Fellowship at Queens' College, Cambridge, UK.

AUTHOR CONTRIBUTIONS

A.M. Rossi, S.C.T., T.R., O.D. and E.J.A.T. completed the biology experiments. V.G.V. performed molecular modeling. A.M. Riley designed and synthesized the ligands and contributed to molecular modeling. B.V.L.P. (chemistry) and C.W.T. (biology) designed and coordinated the project. C.W.T. and A.M. Rossi wrote the manuscript with input from the other authors. All authors discussed the results and commented on the manuscript.

Published online at http://www.nature.com/naturechemicalbiology/.
Reprints and permissions information is available online at http://npg.nature.com/reprintsandpermissions/.

1. Foskett, J.K., White, C., Cheung, K.H. & Mak, D.O. Inositol trisphosphate receptor Ca^{2+} release channels. *Physiol. Rev.* **87**, 593–658 (2007).
2. MacKinnon, R. Potassium channels and the atomic basis of selective ion conduction (Nobel lecture). *Angew. Chem. Int. Edn Engl.* **43**, 4265–4277 (2004).
3. Bosanac, I. *et al.* Structure of the inositol 1,4,5-trisphosphate receptor binding core in complex with its ligand. *Nature* **420**, 696–700 (2002).

4. Uchida, K., Miyauchi, H., Furuichi, T., Michikawa, T. & Mikoshiba, K. Critical regions for activation gating of the inositol 1,4,5-trisphosphate receptor. *J. Biol. Chem.* **278**, 16551–16560 (2003).
5. Szlufcik, K. *et al.* The suppressor domain of inositol 1,4,5-trisphosphate receptor plays an essential role in the protection against apoptosis. *Cell Calcium* **39**, 325–336 (2006).
6. Taylor, C.W., da Fonseca, P.C.A. & Morris, E.P. IP_3 receptors: the search for structure. *Trends Biochem. Sci.* **29**, 210–219 (2004).
7. Lape, R., Colquhoun, D. & Sivilotti, L.G. On the nature of partial agonism in the nicotinic receptor superfamily. *Nature* **454**, 722–727 (2008).
8. Auerbach, A. Gating of acetylcholine receptor channels: Brownian motion across a broad transition state. *Proc. Natl. Acad. Sci. USA* **102**, 1408–1412 (2005).
9. Monod, J., Wyman, J. & Changeux, J.P. On the nature of allosteric transitions: a plausible model. *J. Mol. Biol.* **12**, 88–118 (1965).
10. Colquhoun, D. Binding, gating, affinity and efficacy. *Br. J. Pharmacol.* **125**, 923–947 (1998).
11. Stephenson, R.P. A modification of receptor theory. *Br. J. Pharmacol.* **11**, 379–393 (1956).
12. Jin, R., Banke, T.G., Mayer, M.L., Traynelis, S.F. & Gouax, E. Structural basis for partial agonist action at ionotropic glutamate receptors. *Nat. Neurosci.* **6**, 803–810 (2003).
13. Mayer, M.L. Glutamate receptors at atomic resolution. *Nature* **440**, 456–462 (2006).
14. Banke, T.G. & Traynelis, S.F. Activation of NR1/NR2B NMDA receptors. *Nat. Neurosci.* **6**, 144–152 (2003).
15. Popescu, G. & Auerbach, A. Modal gating of NMDA receptors and the shape of their synaptic response. *Nat. Neurosci.* **6**, 476–483 (2003).
16. Jencks, W.P. Binding energy, specificity, and enzymic catalysis: the circe effect. *Adv. Enzymol. Relat. Areas Mol. Biol.* **43**, 219–410 (1975).
17. Burgen, A.S.V. Conformational changes and drug action. *Fed. Proc.* **40**, 2723–2728 (1981).
18. Potter, B.V.L. & Lampe, D. Chemistry of inositol lipid mediated cellular signaling. *Angew. Chem. Int. Edn Engl.* **34**, 1933–1972 (1995).
19. Riley, A.M., Laude, A.J., Taylor, C.W. & Potter, B.V.L. Dimers of D-*myo*-inositol 1,4,5-trisphosphate: design, synthesis, and interaction with Ins(1,4,5)P_3 receptors. *Bioconjug. Chem.* **15**, 278–289 (2004).
20. Riley, A.M. *et al.* Interactions of inositol 1,4,5-trisphosphate (IP_3) receptors with synthetic poly(ethylene glycol)-linked dimers of IP_3 suggest close spacing of IP_3-binding sites. *J. Biol. Chem.* **277**, 40290–40295 (2002).
21. Kramer, R.H. & Karpen, J.W. Spanning binding sites on allosteric proteins with polymer-linked ligand dimers. *Nature* **395**, 710–713 (1998).
22. Poinas, A. *et al.* Study of the interaction of the catalytic domain of Ins(1,4,5)P_3 3-kinase A with inositol phosphate analogues. *ChemBioChem* **6**, 1449–1457 (2005).
23. Riley, A.M., Dozol, H., Spiess, B. & Potter, B.V.L. 2-*O*-(2-aminoethyl)-*myo*-inositol 1,4,5-trisphosphate as a novel ligand for conjugation: physicochemical properties and synthesis of a new Ins(1,4,5)P_3 affinity matrix. *Biochem. Biophys. Res. Commun.* **318**, 444–452 (2004).
24. Tovey, S.C., Sun, Y. & Taylor, C.W. Rapid functional assays of intracellular Ca^{2+} channels. *Nat. Protoc.* **1**, 258–262 (2006).
25. Takahashi, M., Tanzawa, K. & Takahashi, S. Adenophostins, newly discovered metabolites of *Penicillium brevicompactum*, act as potent agonists of the inositol 1,4,5-trisphosphate receptor. *J. Biol. Chem.* **269**, 369–372 (1994).
26. Dellis, O. *et al.* Ca^{2+} entry through plasma membrane IP_3 receptors. *Science* **313**, 229–233 (2006).
27. Rahman, T.-U., Skupin, A., Falcke, M. & Taylor, C.W. Clustering of IP_3 receptors by IP_3 retunes their regulation by IP_3 and Ca^{2+}. *Nature* **458**, 655–659 (2009).
28. Iwai, M., Michikawa, T., Bosanac, I., Ikura, M. & Mikoshiba, K. Molecular basis of the isoform-specific ligand-binding affinity of inositol 1,4,5-trisphosphate receptors. *J. Biol. Chem.* **282**, 12755–12764 (2007).
29. Yoshikawa, F. *et al.* Mutational analysis of the ligand binding site of the inositol 1,4,5-trisphosphate receptor. *J. Biol. Chem.* **271**, 18277–18284 (1996).
30. Williams, D.H., Zhou, M. & Stephens, E. Ligand binding energy and enzyme efficiency from reductions in protein dynamics. *J. Mol. Biol.* **355**, 760–767 (2006).
31. Boehning, D. & Joseph, S.K. Direct association of ligand-binding and pore domains in homo- and heterotetrameric inositol 1,4,5-trisphosphate receptors. *EMBO J.* **19**, 5450–5459 (2000).
32. Schug, Z.T. & Joseph, S.K. The role of the S4–S5 linker and C-terminal tail in inositol 1,4,5-trisphosphate receptor function. *J. Biol. Chem.* **281**, 24431–24440 (2006).
33. Bosanac, I. *et al.* Crystal structure of the ligand binding suppressor domain of type 1 inositol 1,4,5-trisphosphate receptor. *Mol. Cell* **17**, 193–203 (2005).
34. Chan, J. *et al.* Ligand-induced conformational changes via flexible linkers in the amino-terminal region of the inositol 1,4,5-trisphosphate receptor. *J. Mol. Biol.* **373**, 1269–1280 (2007).
35. Kobilka, B.K. & Deupi, X. Conformational complexity of G-protein-coupled receptors. *Trends Pharmacol. Sci.* **28**, 397–406 (2007).
36. Bosanac, I., Michikawa, T., Mikoshiba, K. & Ikura, M. Structural insights into the regulatory mechanism of IP_3 receptor. *Biochim. Biophys. Acta* **1742**, 89–102 (2004).
37. George, C.H., Jundi, H., Thomas, N.L., Fry, D.L. & Lai, F.A. Ryanodine receptors and ventricular arrhythmias: emerging trends in mutations, mechanisms and therapies. *J. Mol. Cell. Cardiol.* **42**, 34–50 (2007).
38. Wagenknecht, T. & Samsó, M. Three-dimensional reconstruction of ryanodine receptors. *Front. Biosci.* **7**, 1464–1474 (2002).
39. Marwood, R.D., Correa, V., Taylor, C.W. & Potter, B.V.L. Synthesis of adenophostin A. *Tetrahedron Asymmetry* **11**, 397–403 (2000).
40. Riley, A.M. *et al. Scyllo*-inositol pentakisphosphate as an analogue of *myo*-inositol 1,3,4,5,6-pentakisphosphate: chemical synthesis, physicochemistry and biological applications. *ChemBioChem* **7**, 1114–1122 (2006).
41. Sugawara, H., Kurosaki, M., Takata, M. & Kurosaki, T. Genetic evidence for involvement of type 1, type 2 and type 3 inositol 1,4,5-trisphosphate receptors in signal transduction through the B-cell antigen receptor. *EMBO J.* **16**, 3078–3088 (1997).
42. Cardy, T.J.A., Traynor, D. & Taylor, C.W. Differential regulation of types 1 and 3 inositol trisphosphate receptors by cytosolic Ca^{2+}. *Biochem. J.* **328**, 785–793 (1997).
43. Yoshikawa, F. *et al.* High efficient expression of the functional ligand binding site of the inositol 1,4,5-trisphosphate receptor in *Escherichia coli*. *Biochem. Biophys. Res. Commun.* **257**, 792–797 (1999).
44. Jiang, Q.-X., Thrower, E.C., Chester, D.W., Ehrlich, B.E. & Sigworth, F.J. Three-dimensional structure of the type 1 inositol 1,4,5-trisphosphate receptor at 24 Å resolution. *EMBO J.* **21**, 3575–3581 (2002).
45. Colquhoun, D. *Lectures in Biostatistics* 279–343 (Clarendon Press, Oxford, 1971).
46. Ritchie, D.W., Kozakov, D. & Vajda, S. Accelerating and focusing protein-protein docking correlations using multi-dimensional rotational FFT generating functions. *Bioinformatics* **24**, 1865–1873 (2008).
47. Gray, J.J. *et al.* Protein-protein docking with simultaneous optimization of rigid-body displacement and side-chain conformations. *J. Mol. Biol.* **331**, 281–299 (2003).
48. Riley, A.M., Correa, V., Mahon, M.F., Taylor, C.W. & Potter, B.V.L. Bicyclic analogues of D-myo-inositol 1,4,5-trisphosphate related to adenophostin A: synthesis and biological activity. *J. Med. Chem.* **44**, 2108–2117 (2001).
49. Riley, A.M., Guédat, P., Schlewer, G., Spiess, B. & Potter, B.V.L. A conformationally restricted cyclic phosphate analogue of inositol trisphosphate: synthesis and physicochemical properties. *J. Org. Chem.* **63**, 295–305 (1998).
50. Riley, A.M. & Potter, B.V.L. Poly(ethylene glycol)-linked dimers of D-*myo*-inositol 1,4,5-trisphosphate. *Chem. Commun. (Camb.)* 983–984 (2000).

Supplementary Information

Synthetic partial agonists reveal key steps in IP_3 receptor activation

Ana M. Rossi[1], Andrew M. Riley[2], Stephen C. Tovey[1], Taufiq Rahman[1], Olivier Dellis[1], Emily J. A. Taylor[1], Valery G. Veresov[3], Barry V. L. Potter[2] & Colin W. Taylor[1]

[1]Department of Pharmacology, University of Cambridge, Tennis Court Road, Cambridge, CB2 1PD, UK; [2]Wolfson Laboratory of Medicinal Chemistry, Department of Pharmacy and Pharmacology, University of Bath, Claverton Down, Bath, BA2 7AY, UK; [3]Department of Cell Biophysics, Institute of Biophysics and Cell Engineering, Minsk 220072, Academicheskaya St. 27, Belarus.

This pdf file includes:

Nature Chemical Biology: doi:10.1038/nchembio.195

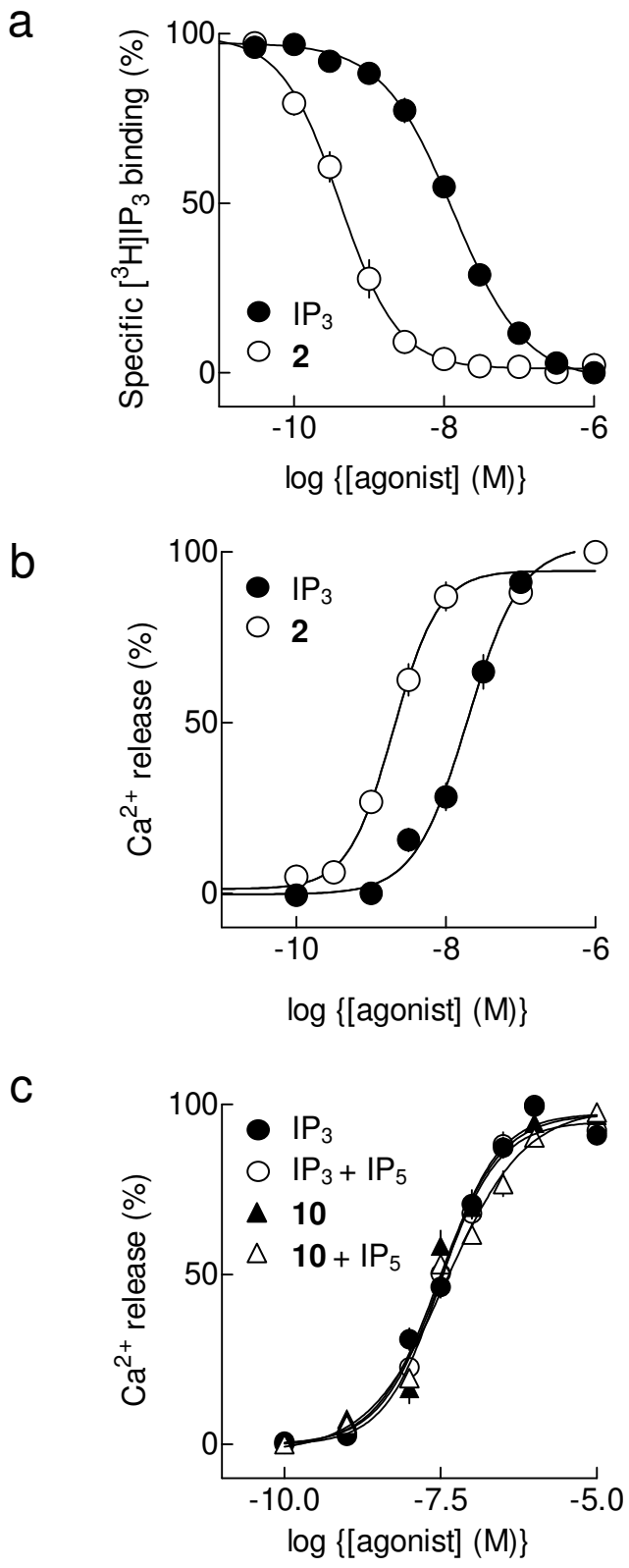

Supplementary Figure 1 2-*O*-modified IP_3 analogues are high-affinity agonists of IP_3R1. (**a**) Equilibrium competition binding to purified IP_3R1 with ^3H-IP_3 and IP_3 or **2**; n ≥ 8. Specific ^3H-IP_3 binding is shown in the presence of the indicated concentrations of competing ligands. (**b**) Ca^{2+} release from permeabilized DT40-IP_3R1 cells evoked by IP_3 or **2**; n = 4-5. Ca^{2+} release is expressed as a percentage of that released by a maximally effective concentration. (**c**) IP_5 does not affect the Ca^{2+} release evoked by IP_3 or **10**. Permeabilized DT40-IP_3R1 cells were stimulated with the indicated concentrations of IP_3 or **10** alone or after pre-incubation (30s) with 10μM IP_5, which alone did not evoke Ca^{2+} release; n = 6. All results are means ± SEM.

Nature Chemical Biology: doi:10.1038/nchembio.195

a

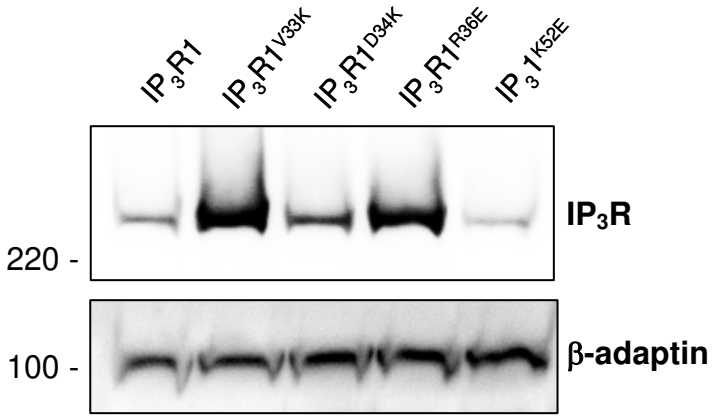

b

	IP_3R1	IP_3R1^{V33K}	IP_3R1^{D34K}	IP_3R1^{R36E}	IP_3R1^{K52E}
Expression, %	100	290 ± 30	140 ± 20	190 ± 30	70 ± 20

c

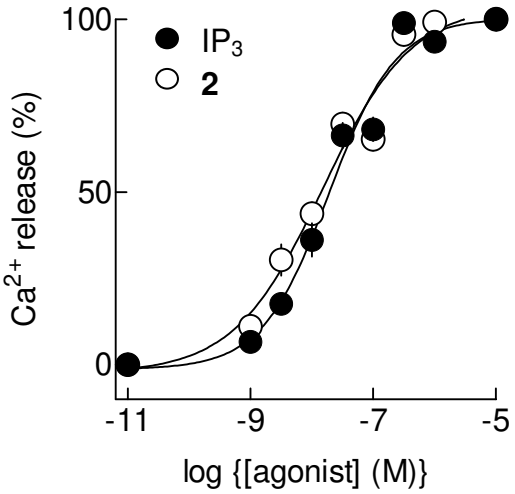

Supplementary Figure 2 Expression of IP_3R and its mutants in DT40 cells. (**a**) Lanes were loaded with lysate (75μg protein) from DT40 cells expressing IP_3R1 and the indicated mutants, and then immunoblotted with Ab1.3 (top panel) or β-adaptin (bottom). Molecular weights (kDa) are shown on the left. (**b**) From 4 similar blots, IP_3R1 expression (corrected for β-adaptin loading) is shown for each mutant as a % of expression in DT40-IP_3R1 cells (means ± SEM). These results demonstrate that the cells used to examine the effects of mutations within the SD on Ca^{2+} release evoked by IP_3 and **2** (**Fig. 4**) differed by no more than 3-fold from DT40-IP_3R1 cells in their levels of IP_3R expression. Although the level of IP_3R expression does affect the absolute sensitivity of the intracellular Ca^{2+} stores to IP_3, the effect on EC_{50} appears to be substantially less than the change in expression level. Our previous work, for example, showed that a >20-fold increase in IP_3R1 expression caused the EC_{50} for IP_3 to decrease by only ~2.5-fold[26]. In any event, we use the cells expressing mutant IP_3R only to compare the responses to IP_3 and **2** *within* each cell line, and not for comparisons of responses between cell lines (see **Supplementary Table 4**). (**c**) Ca^{2+} release from permeabilized DT40-IP_3R1^{V33K} cells in response to IP_3 or **2**; n ≥ 5. Results are means ± SEM**.**

Nature Chemical Biology: doi:10.1038/nchembio.195

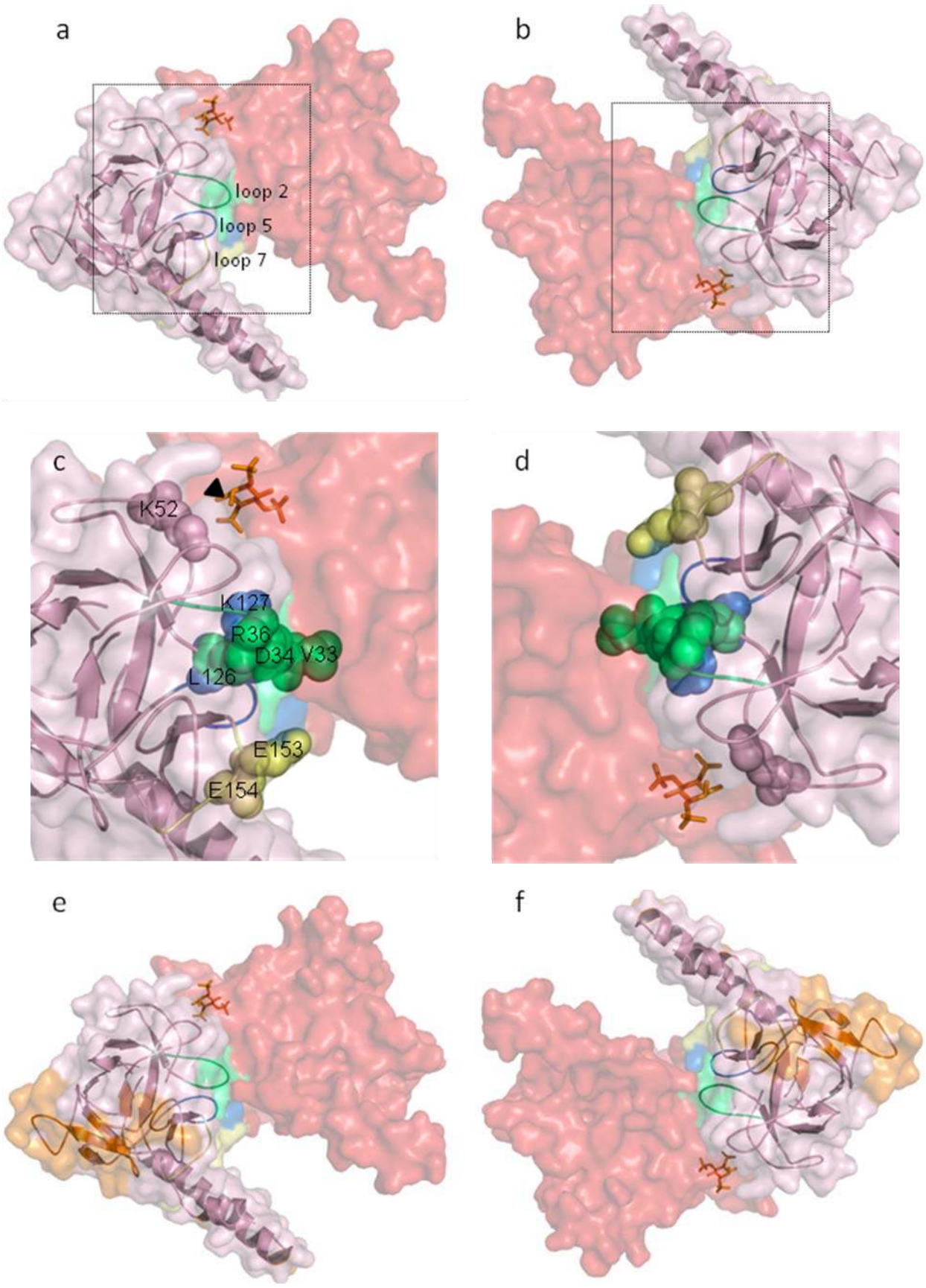

Supplementary Figure 3 Proposed structural relationship of the SD and IBC. (**a,b**) The proposed arrangement of the SD (pink) and IBC (red) is shown (see **Supplementary Methods**) to highlight residues implicated in their interaction; b is the view shown in panel a

Nature Chemical Biology: doi:10.1038/nchembio.195

rotated by 180°. Analysis of subtype-specific interactions of the SD and IBC of IP_3R1 and IP_3R3 established that exposed loops linking the β5-β6 (loop 5, blue) and β7-β8 regions (loop 7, yellow) of the SD determined its subtype-specific interactions with the IBC[28]. Within loop 5, only one residue (L126 in IP_3R1) differs between IP_3R1 and IP_3R3; and within loop 7 there are three differences (E153, A154 and F161), one of which (F161L) is a rather conservative change. These results suggest that L126 from loop 5 of the SD and either or both of E153 and A154 from loop 7 interact directly with the IBC. Our model shows each of these residues to be present at the putative SD-IBC interface. The mutations (V33K, D34K, R36E and K127E) that reduced efficacy by perturbing the SD-IBC interaction also lie at the SD-IBC interface. The ineffective mutation (K52) is not part of this interface. The dimensions of our proposed structure are compatible also with the results from small angle X-ray scattering[34]. The SD-IBC arrangement proposed by Chan *et al*.[34] is less appealing in that it does not provide an explanation for the subtype-specific interactions between the SD and IBC[28], because the key SD residues do not contact the IBC. (**c,d**) Enlargements of the boxed areas in panels a and b. The 2-OH of IP_3 is indicated by an arrow. (**e,f**) Residues conserved between IP_3R and RyR are highlighted in orange. We suggest that this surface might signal onwards from the SD towards the pore (see text).

Nature Chemical Biology: doi:10.1038/nchembio.195

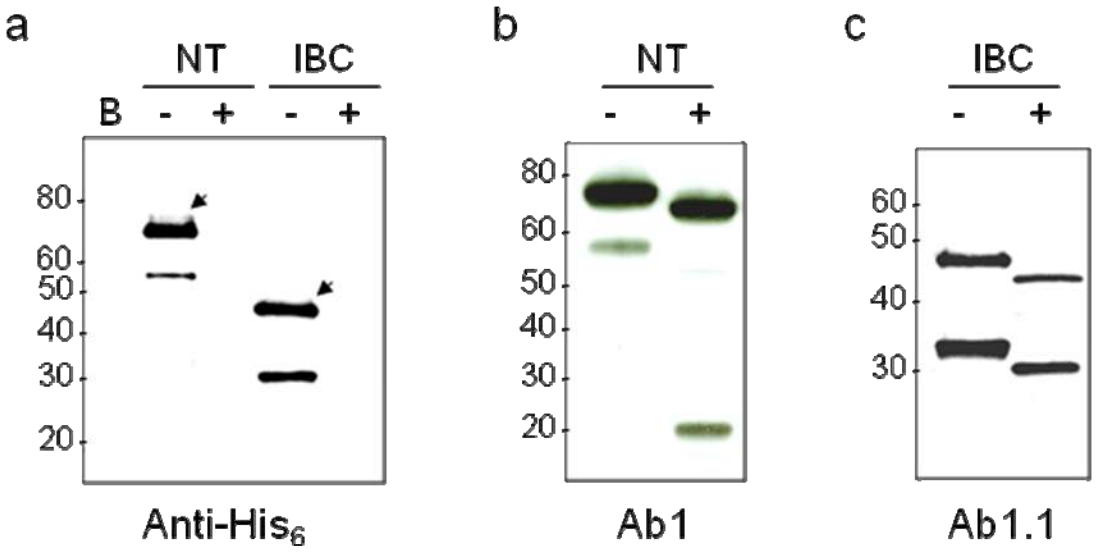

Supplementary Figure 4 Expression of N-terminal fragments of IP_3R. An N-terminal His_6-tag was reported[43] to have no effect on IP_3 binding to the NT (although the same authors[28] subsequently avoided His_6-tags). We found the tag to reduce substantially the affinity for IP_3 of both the IBC and the NT. The K_d was 82.9 ± 13.0nM and 2.82 ± 0.26nM for His_6-NT and NT, respectively; and 1.41 ± 0.38nM and 0.21 ± 0.03nM for His_6-IBC and IBC, respectively. The effect of the His_6 tag is, however, entirely different from that of the SD. The SD selectively attenuated IP_3 relative to **2** binding to the IBC (**Fig. 3a**), whereas the His_6 tag similarly inhibited both (K_d = 1.14 ± 0.39 and 0.21 ± 0.06nM for **2** binding to IBC with and without His_6). We failed to remove His_6-tags using an enterokinase-cleavage site, but were successful with an engineered thrombin-cleavage site (see **Methods**).

Fragments of IP_3R1 (NT, residues 1-604; IBC, 224-604) with N-terminal His_6 tags were expressed in *E. coli* and prepared for immunoblotting before (-) or after (+) incubation with thrombin to remove the His_6 tags. (**a**) Immunoblot of bacterial lysates using an anti-His_6 antibody (Anti-His_6) identified bands of the expected masses (arrows) and a smaller band associated with each product. The His_6-reactive bands were absent after thrombin-digestion. B denotes lysate from untransformed bacteria. (**b**, **c**) Immunoblots of bacterial lysates before (-) and after (+) treatment with thrombin, followed by immunostaining with antisera selective for IP_3R1: Ab1 (**b**) or Ab1.1 (**c**). The bands of lower molecular mass are unlikely to bind IP_3 because, unlike the upper bands, they do not bind to heparin, a competitive antagonist of IP_3 (not shown). In analyses of IP_3 binding, bacterial lysates treated with thrombin to remove the His_6 tag were used without further purification. Under these conditions the fragments are monomeric. His_6-tagged and GST-tagged NT fragments did not co-precipitate when incubated in equal amounts and subjected to immunoprecipitation with either Anti-His_6 or Ab-GST (not shown). Positions of molecular weight markers (kDa) are shown to the left of each blot.

Nature Chemical Biology: doi:10.1038/nchembio.195

Supplementary Table 1. Single channel properties of IP_3R1 activated by full and partial agonists. The results (means ± SEM (*n*)) are from experiments similar to those shown in **Fig. 2b**. All ligands were included in the pipette at a final concentration of 10μM. ND, not determined.

When P_o is low, it requires long recordings to be confident of the number of IP_3R within a patch. For example[27], with an estimated P_o of 0.08 and τ_o of 10ms for **2**, we need (with $p < 0.05$) to record for >35s to establish whether ≥2 IP_3R are present within a patch. Our recordings with partial agonists typically lasted for 8-10min, which is more than sufficient time to establish whether a patch contains only a single IP_3R. The table (and figures) show only results from patches with a single IP_3, thereby allowing P_o (the single channel open probability) to be determined reliably.

	P_o	γ_K, pS	τ_o, ms	τ_c, ms
IP_3	0.50 ± 0.02 (*4*)	216 ± 22 (*3*)	9.1 ± 0.8 (*4*)	9.2 ± 1 (*4*)
AdA	0.52 ± 0.04 (*3*)	209 ± 4 (*3*)	12.2 ± 1.3 (*3*)	11.8 ± 3 (3)
2	0.12 ± 0.05 (*3*)	230 ± 35 (*3*)	9.8 ± 0.47 (*3*)	69.9 ± 21.5 (*3*)
6	0.18 ± 0.05 (*4*)	221 ± 8 (*3*)	13.2 ± 1.9 (*4*)	76.5 ± 20 (*4*)
9	0.22 ± 0.05 (*5*)	204 ± 13 (*3*)	10.6 ± 1.4 (*4*)	59.5 ± 26.6 (*4*)
10	0.50 ± 0.06 (*4*)	193 ± 21 (*3*)	9.8 ± 0.99 (*3*)	8.1 ± 1.3 (*4*)
IP_3 with **2**	0.20 ± 0.033 (*4*)	ND	11.8 ± 0.63 (*4*)	56.5 ± 16.4 (*4*)

Nature Chemical Biology: doi:10.1038/nchembio.195

Supplementary Table 2. ΔG for ligand-evoked rearrangement of the SD. Binding affinities of ligands for the IBC, NT and full-length IP_3R1 (FL) are shown, with ΔG calculated from: $\Delta G = RT ln K_d$. ΔΔG, the difference between ΔG for the NT (or FL) and IBC, reflects a component of the binding energy used to drive rearrangements of the protein. Hence ΔΔG(IBC-NT) represents the binding energy used to rearrange the SD; and ΔΔG(IBC-FL) represents the binding energy used to change the conformation of the entire IP_3R. See text and **Table 1** for details. The bottom rows (shaded) show ΔG for IP_3 binding to each of the three IP_3R subtypes, calculated from the results in[28], which were performed under conditions that differed from our binding analyses, but which nevertheless confirm that the SD reduces the affinity of the IBC for IP_3 by ~5-10kJ/mol.

	Ligand	**ΔG IBC** kJ/mol	**ΔG NT** kJ/mol	**ΔG FL** kJ/mol	**ΔΔG IBC–NT** kJ/mol	**ΔΔG IBC–FL** kJ/mol
1	IP_3	-51.4	-45.4	-41.9	-6	-9.5
2	$(IP_3)_2$ 0.8nm	-51.7	-49.8	-49.6	-1.9	-2.1
3	$(IP_3)_2$ 1.5nm	-51.7	-49.5	-48.1	-2.2	-3.6
4	$(IP_3)_2$ 8nm	-49.5	-47.0	-47.0	-2.4	-2.5
5	IP_3–L-IP_3 0.8nm	-52.3	-49.8	-48.0	-2.5	-4.3
6	IP_3–IP_5 0.8nm	-51.5	-50.1	-48.0	-1.4	-3.4
7	IP_3–Ins 0.8nm	-50.3	-45.4	-43	-4.9	-7.3
9	2-adamantane-IP_3	-51.5	-46.6	-43.1	-4.9	-8.4
10	2-deoxy-IP_3	-51.2	-44.6	-41.2	-6.6	-10.0
11	2-aminoethyl-IP_3	-49.3	-41.8	-39.1	-7.5	-10.2
IP_3	IP_3R1	-44.4	-37.1	-35.2	-7.3	-9.2
IP_3	IP_3R2	-44.8	-39.9	-36.6	-4.9	-8.2
IP_3	IP_3R3	-44.1	-34.5	-31.7	-9.6	-12.4

Nature Chemical Biology: doi:10.1038/nchembio.195

Supplementary Table 3. Binding of IP_3 and **2** to NT with mutated SD. Results show K_d (nM) for each ligand determined from equilibrium competition binding with ^3H-IP_3. Means ± SEM from n ≥ 5 independent experiments. The positions of the mutations in the SD structure are shown in **Figure 4a**.

Fragment	IP_3	**2**
NT	2.32 ± 0.35	0.56 ± 0.04
IBC	0.20 ± 0.09	0.21 ± 0.06
NT^{V33K}	0.27 ± 0.10	0.27 ± 0.16
NT^{D34K}	0.98 ± 0.22	0.68 ± 0.18
NT^{R36E}	0.46 ± 0.13	0.40 ± 0.20
NT^{K127E}	0.45 ± 0.08	0.32 ± 0.02
NT^{K52E}	2.64 ± 0.37	0.78 ± 0.08

Supplementary Table 4. Responses of IP_3R1 with mutations in the SD to IP_3 and **2**. Results show the EC_{50} for Ca^{2+} release evoked by IP_3 or **2** in permeabilized DT40 cells expressing IP_3R1 with the indicated point mutations within the SD. The fraction of the stores (70-80%) released by maximal concentrations of IP_3 and **2** were the same in each cell line and between cell lines. Means ± SEM, from n ≥ 5 independent experiments. The comparisons are between stable cell lines in which IP_3R expression levels are not identical (**Supplementary Fig. 2a,b**). Because the EC_{50} for IP_3-evoked Ca^{2+} release can be affected by IP_3R expression level[26], absolute differences in EC_{50} values between cell lines are of less value than the ratio of EC_{50} values for different ligands within each cell line (final column). We were unable, despite repeated attempts, to generate a stable DT40 cell line expressing IP_3R1^{K127E}.

	EC_{50}, nM		**EC_{50} ratio**
	IP_3	**2**	IP_3 / **2**
IP_3R1	35.4 ± 3.8	2.9 ± 0.43	12.2 ± 2.2
IP_3R1^{V33K}	22.3 ± 6.2	19.5 ± 1.7	1.1 ± 0.3
IP_3R1^{D34K}	26.6 ± 11.9	11.5 ± 4.9	2.3 ± 1.4
IP_3R1^{R36E}	40.8 ± 6.1	15.8 ± 3.6	2.6 ± 0.7
IP_3R1^{K52E}	85.0 ± 8.2	7.7 ± 1.3	11.0 ± 2.1

Nature Chemical Biology: doi:10.1038/nchembio.195

Supplementary Table 5. Primers used to generate IP_3R1 and the NT and IBC fragments (5′-3′). The codes are those used in the **Methods** section.

Primer	Sequence
P1	AACGTCGACCTGGTTCCGCGTGGATCCATGTCTGACAAA TGTCTAGT
P2	CTGGAATTCTCACTTTCGGTTGTTGTGGAGCAGGGCAGT GATGGTGTC
P3	AACCTCGAGCTGGTTCCGCGTGGATCCATGAAATGGAGT GATAACAAA
P4	ATTACTTGGCAGCAGAGGTAGACCCTGACTTTGAGGAAG AATGCCTGGAGT TTCAGCCCTCAGTGGACCCTGATCAGG
P5	GATCAGGGTCCACTGAGGGCTGAAACTCCAGGCATTCTT CCTCAAAGTCAGGGTCTACCTCTGC TGCCAAGTAATGC
P6	AGGAATTCGCCACCATGTCTGACAAAATG
P7	CCGGTACCGAATTCTTAGGCTGGCTGCTGT

Supplementary Table 6. Primers used to introduce mutations into the SD (5′-3′). Codons for mutated residues are highlighted.

Mutation		Primers
V33K	Forward	AGCACCTTGGGCTTG**AAA**GATGACCGTTGCGTT
	Reverse	AACGCAACGGTCATC**TTT**CAAGCCCAAGGTGCT
D34K	Forward	ACCTTGGGCTTGGTT**AAA**GACCGTTGCGTTGTA
	Reverse	TACAACGCAACGGTC**TTT**AACCAAGCCCAAGGT
R36E	Forward	GGCTTGGTTGATGAC**GAA**TGCGTTGTACAGCCA
	Reverse	TGGCTGTACAACGCA**TTC**GTCATCAACCAAGCC
K52E	Forward	AACAATCCACCCAAG**GAA**TTCAGAGACTGCCTC
	Reverse	GAGGCAGTCTCTGAA**TTC**CTTGGGTGGATTGTT
K127E	Forward	CAGCTCCTACATTTG**GAA**AGCAATAAATACTTA
	Reverse	TAAGTATTTATTGCT**TTC**CAAATGTAGGAGCTG

Nature Chemical Biology: doi:10.1038/nchembio.195

SUPPLEMENTARY METHODS

Supplementary biological methods

Antibodies
Polyclonal Ab1 antiserum[42] was raised to a peptide comprising residues 62-75 of rat IP_3R1. Polyclonal Ab1.1 antiserum was raised to a peptide comprising residues 318-332 (S1 splice site) of rat IP_3R1. Polyclonal Ab1.3 antiserum[42] was raised to a peptide derived from residues 2733-2749 of rat IP_3R1. All IP_3R primary antisera were used at 1:1000 dilution. Anti-β-adaptin antiserum was from Santa Cruz (1:2000). The anti-His_6 antibody was from Sigma (1:3000). The HRP-conjugated secondary antibodies used were anti-mouse (1:1000, Sigma), anti-rabbit (1:5000, Santa Cruz) and anti-goat (1:2000, Santa Cruz).

Molecular modelling
A protein-protein docking approach was used to develop a model of the IBC-SD complex using coordinate files for the IBC (1N4K) and SD (1XZZ). First, the program Hex5.1 (http://www.csd.abdn.ac.uk/hex/)[46] was used to generate coarse-grained models of the IBC-SD complex. For this initial rigid-body docking, two short loops that extend into the ARM-β_2 cleft of the IBC (linking β-strands 3-4 and 10-11) and another within the SD (linking β-strands 2-3) were removed to avoid rejecting models because of steric clashes between the flexible loops. From ~100 structures generated by Hex5.1, several were rejected because they were incompatible with there being only 11 residues between the linked termini of the SD (L224) and IBC (G236). Of the remaining structures, only two clusters placed residues within the SD that determine its subtype-specific interactions with the IBC (Ref. 28) (**Supplementary Fig. 3**) at an interface between the IBC and SD. In only one of these clusters was the SD close enough to the IP_3-binding site to approach the second IP_3 moiety of **2** bound to the IBC. A representative structure from this cluster was further refined using a local docking search with RosettaDock[47], which allows for side-chain flexibility. Finally, the missing loops were restored and the IBC-SD complex was subject to local minimization using the program SE (Ref. 51), adapted to the force field ECEPP/2/3 (Refs. 52,53).

Analysis of single channel records
QuB (www.qub.buffalo.edu) was used for analysis of all channel records. Currents were typically recorded at a holding potential of +40mV and further filtered offline (500Hz) for display. When the pipette solution contained a free $[Ca^{2+}]$ (200nM) that mimicked that of a resting cell, the activity of nuclear IP_3R1 stimulated by either IP_3 (10μM) or AdA (0.5μM) was reasonably high ($P_o \sim 0.5$, **Supplementary Table 1**), allowing a robust kinetic analysis of the observed dwell time distributions. These are compatible with kinetic schemes consisting of two closed states linearly connected to a single open state[27]. However, with the partial agonists or for IP_3R1^{V33K}, P_o was much reduced ($P_o \leq 0.1$, **Supplementary Table 1**). We have not yet, therefore, subjected these records to the same detailed analysis. Under all conditions, we detected a single open state, which had the same τ_o for each agonist (**Supplementary Table 1**). This allowed us to consider a simplified gating scheme (closed↔open) (**Fig. 2e**), where τ_c is simply the average duration of all closed events calculated from:

$$\tau_c = \sum_{i=1}^{n} (a_i \times \tau_i) \text{ (Ref. 54)}$$

where a_i is the fractional area occupied by the i^{th} component in the distribution such that the areas corresponding to all components add up to unity, and τ_i is the time constant for the i^{th} component.

Nature Chemical Biology: doi:10.1038/nchembio.195

Synthetic procedures and compound characterization

General methods

Tetrahydrofuran (THF) was distilled from sodium and benzophenone under a nitrogen atmosphere. Dimethylformamide (DMF), acetonitrile and dichloromethane were purchased in anhydrous form and used without further purification. Triethylamine used in conjugation reactions was dried over KOH, distilled and kept over KOH. Bis(4-nitrophenyl) carbonate was recrystallised from CH_2Cl_2:hexane. D-2-*O*-(2-aminoethyl)-IP_3 (**11**)[23] was synthesized as previously reported and used as the triethylammonium salt. ^1H, ^{13}C, ^{31}P and ^{19}F NMR spectra were collected on either a JEOL Delta machine at 270 MHz (^1H), 68 MHz (^{13}C), or 109 MHz (^{31}P) or a Varian Mercury VX machine at 400 MHz (^1H), 100 MHz (^{13}C) 162 MHz (^{31}P) or 376 MHz (^{19}F). NMR spectral assignments, where given, are based on ^1H–^1H COSY, gHMQC, 135DEPT and PENDANT experiments. Low-resolution FAB mass spectra were recorded on a Micromass Autospec instrument on samples in a *m*-nitrobenzyl alcohol matrix at the Mass Spectrometry Centre, University of Bath. Electrospray (ES) HRMS data were recorded with a Bruker micrOTOF-Focus instrument. Elemental analyses were performed by the Microanalysis Service, University of Bath. Thin-layer chromatography (TLC) was performed on precoated plates (Merck TLC aluminium sheets silica 60 F_{254}) with detection by UV light or with phosphomolybdic acid in methanol or alkaline aqueous $KMnO_4$, followed by heating. "NH_4OH" refers to an approximately 28% w/w solution of NH_3 in water. Flash chromatography was carried out on silica (particle size 35–70 μm). All target polyphosphates were purified by ion exchange chromatography on Q-Sepharose Fast Flow using a Pharmacia Biotech Gradifrac system with a P-1 pump, eluting with gradients of triethylammonium bicarbonate (TEAB) buffer and using H_2O of MilliQ quality. Phosphate-containing fractions were identified using a modification of the Briggs phosphate test[55] and the target polyphosphates were accurately quantified using the Ames phosphate assay[56].

Nature Chemical Biology: doi:10.1038/nchembio.195

Syntheses of L-IP_3 homo-dimer (8) and IP_3–L-IP_3 hetero-dimer (5)

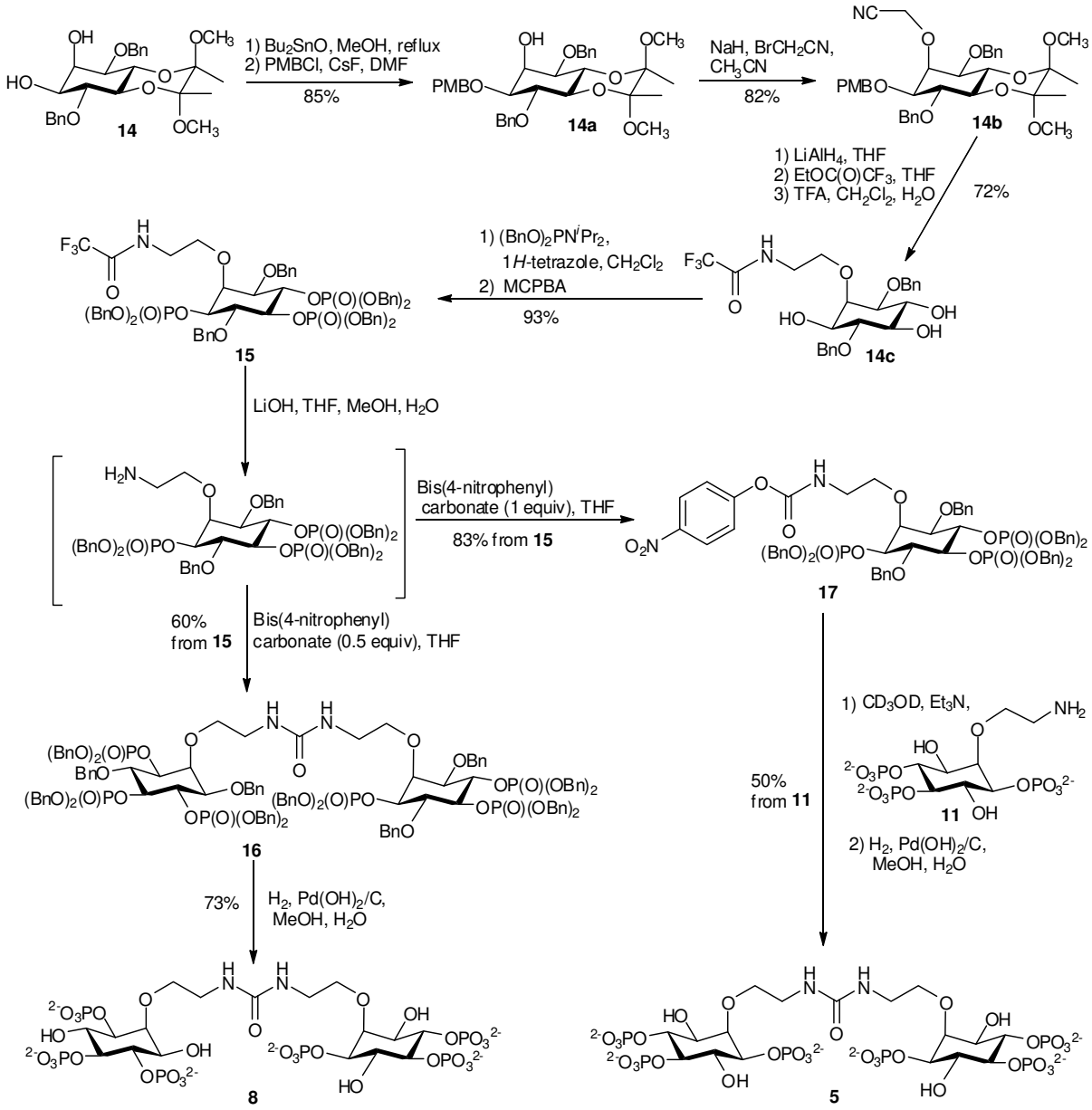

(2′*R*,3′*R*)-D-1,4-di-*O*-benzyl-5,6-*O*-(2′,3′-dimethoxybutane-2′,3′-diyl)-3-*O*-(4-methoxybenzyl)-*myo*-inositol (14a)

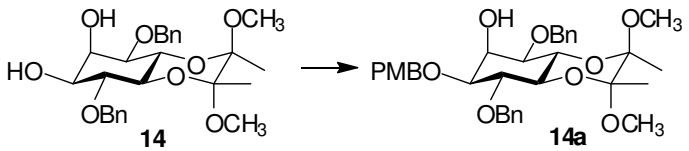

To a solution of (2′*R*,3′*R*)-1D-1,4-di-*O*-benzyl-5,6-*O*-(2′,3′-dimethoxybutane-2′,3′-diyl)-*myo*-inositol (**14**)[48] (2.79 g, 5.88 mmol) in MeOH (150 mL) was added dibutyltin oxide (1.48 g, 5.94 mmol). The suspension was heated at reflux for 16 h with removal of formed water using a Soxhlet apparatus containing 3 Å molecular sieves. The resulting clear solution was

Nature Chemical Biology: doi:10.1038/nchembio.195

allowed to cool and then concentrated to dryness by evaporation under reduced pressure. CsF (1.79 g, 11.8 mmol, previously dried *in vacuo* over P_2O_5) was added and the flask was fitted with a rubber septum and N_2 line. Anhydrous DMF (30 mL) was injected, followed by 4-methoxybenzyl chloride (0.95 mL, 7.1 mmol) and the mixture was stirred at 50 ºC under N_2 for 3 h, after which time TLC ($CHCl_3$:acetone, 30:1 v/v) showed almost total conversion of diol (R_f = 0.15) into a product (R_f = 0.36). The solvents were removed by evaporation *in vacuo* at 50 ºC and the residue was taken up in Et_2O (100 mL) and washed with water (100 mL). The organic layer was dried over $MgSO_4$, filtered through Celite and concentrated by evaporation under reduced pressure to give an oily residue. Purification by flash chromatography (Et_2O:hexane 1:2, then 1:1 v/v) gave alcohol **14a** as a white foam (2.97 g, 5.00 mmole, 85%); TLC (Et_2O:hexane, 2:1 v/v): R_f = 0.32; TLC ($CHCl_3$:acetone, 30:1 v/v): R_f = 0.36; $[\alpha]_D$ = −70 (c = 1.4% w/v in $CHCl_3$) [lit.[19] $[\alpha]_D$ = +69 (c = 1.3% w/v in $CHCl_3$) for the enantiomer]; ^{1}H and ^{13}C NMR spectra of **14a** were identical to those previously reported for the enantiomer[19]; HRMS (m/z) $[M+Na]^+$ calcd. for $C_{34}H_{42}O_9$, 617.2721; found 617.2714; analysis (calcd., found for $C_{34}H_{42}O_9$): C (68.67, 68.4), H (7.12, 7.15).

(2′*R*,3′*R*)-D-1,4-di-*O*-benzyl-2-*O*-cyanomethyl-5,6-*O*-(2′,3′-dimethoxybutane-2′,3′-diyl)-3-*O*-(4-methoxybenzyl)-*myo*-inositol (14b)

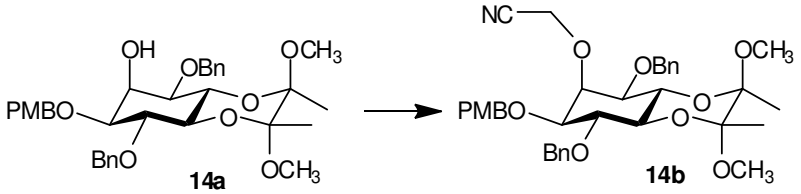

To a solution of **14a** (2.40 g, 4.04 mmole) in dry acetonitrile (10 mL) was added sodium hydride (0.80 g of a 60% dispersion in mineral oil, 20 mmole). The suspension was stirred under N_2 at room temperature for 1 h and then cooled to –40 ºC using an acetonitrile/dry ice cooling bath. Bromoacetonitrile (1.5 mL, 22 mmole) was added dropwise, and stirring was continued at –40 ºC to –20 ºC for 5 h. The suspension was then allowed to warm to room temperature and stirring was continued overnight. The resulting brown liquid was concentrated by evaporation under reduced pressure and the residue was suspended in water (100 mL), and extracted with Et_2O (2 × 100 mL). The combined organic extracts were dried over $MgSO_4$ and concentrated to give a brown residue. Purification by flash chromatography (Et_2O:hexane, 2:3 v/v) gave the product **14b** as a white solid (2.09 g, 3.30 mmole, 82 %); mp: 118.5–119.5 ºC (from ethyl acetate:hexane); TLC (Et_2O:hexane, 1:1 v/v): R_f = 0.26; $[\alpha]_D$ = –57 (c = 1.0% w/v in $CHCl_3$) [lit.[19] $[\alpha]_D$ = +56 (c = 1.0% w/v in $CHCl_3$) for the enantiomer]; ^{1}H and ^{13}C NMR spectra of **14b** were identical to those previously reported for the

Nature Chemical Biology: doi:10.1038/nchembio.195

enantiomer[19]; HRMS (*m*/*z*) $[M+Na]^+$ calcd. for $C_{36}H_{43}NO_9$, 656.2830; found 656.2812; analysis (calcd., found for $C_{36}H_{43}NO_9$): C (68.23, 68.2), H (6.84, 6.85), N (2.21, 2.10).

D-1,4-di-*O*-benzyl-2-*O*-[2-(2,2,2-trifluoroacetylamino)ethyl]-*myo*-inositol (14c)

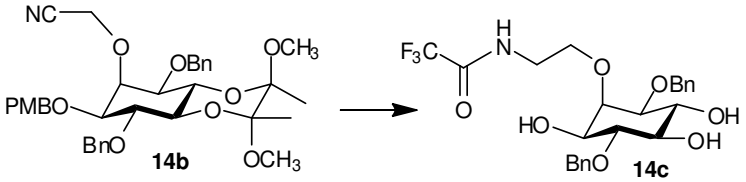

To a solution of $LiAlH_4$ in THF (3.0 mL of a 1 $moldm^{-3}$ solution, 3.0 mmol) under N_2 at room temperature was added a solution of **14b** (1.90 g, 3.00 mmol) in dry THF (5 mL) dropwise over 10 min. The mixture was stirred at room temperature for a further 1 h and then quenched by careful addition of water. 15% w/v aq. NaOH (50 mL) was added and the resulting solution was extracted with CH_2Cl_2 (3 × 50 mL). The combined organic extracts were dried ($MgSO_4$) and concentrated to give the crude amine (~2 g) as a colorless oil. The crude amine was taken up in dry THF (5 mL) and ethyl trifluoroacetate (0.5 mL, 4.2 mmol) was added. The solution was stirred at room temperature with exclusion of moisture overnight and then concentrated by evaporation under reduced pressure to give an oil, which was redissolved in CH_2Cl_2 (10 mL). Aqueous trifluoroacetic acid (95 % v/v, 10 mL) was added and the solution was stirred at room temperature for 30 min, then concentrated by evaporation under reduced pressure. The residue was purified by flash chromatography (EtOAc:hexane, 2:1 v/v) to give triol **14c** as a white solid (1.08 g, 2.16 mmole, 72 % yield over three steps); mp: 129–131 °C (from EtOAc:hexane); TLC (CH_2Cl_2:MeOH, 20:1 v/v): R_f = 0.20; $[\alpha]_D$ = –3 (*c* = 1.0% w/v in $CHCl_3$) [lit.[19] $[\alpha]_D$ = +3 (*c* = 1.0% w/v in $CHCl_3$) for the enantiomer]; ^1H and ^{13}C NMR spectra of **14c** were identical to those previously reported for the enantiomer[19]; HRMS (*m*/*z*) $[M]^+$ calcd. for $C_{24}H_{28}F_3NO_7$, 500.1891; found 500.1878; analysis (calcd., found for $C_{24}H_{28}F_3NO_7$): C (57.71, 57.8), H (5.65, 5.57), N (2.80, 2.70).

D-1,4-di-*O*-benzyl-2-*O*-[2-(2,2,2-trifluoroacetyl)aminoethyl]-*myo*-inositol 3,5,6-tris(dibenzylphosphate) (15)

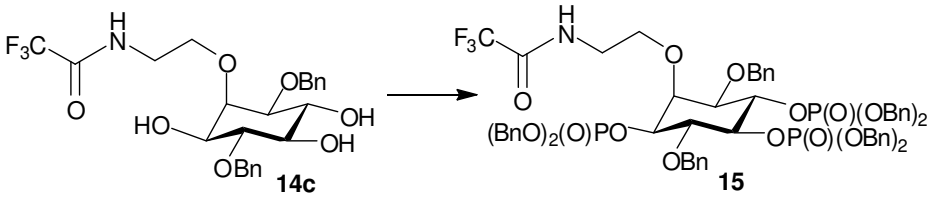

To a suspension of 1*H*-tetrazole (250 mg 3.57 mmol) and triol **14c** (300 mg, 0.601 mmol) in dry CH_2Cl_2 (5 mL) under N_2 was added bis(benzyloxy)diisopropylaminophosphine (0.9 mL, 2.68 mmol). The mixture was stirred at room temperature for 1.5 h and then cooled to –78 ºC, before MCPBA (57%, 1.1 g, 3.6 mmol) was added in portions over 1 min. The mixture was

Nature Chemical Biology: doi:10.1038/nchembio.195

allowed to warm to room temperature and then diluted with CH_2Cl_2 (50 mL). The clear solution was washed with 10% aq. Na_2SO_3 solution (50 mL), dried over $MgSO_4$ and concentrated. The residue was purified by flash chromatography (EtOAc:hexane 1:1 then 2:1 v/v) to give **15** as an oil, which slowly crystallized (715 mg, 0.559 mmole, 93%); mp: 85–87 °C (from diisopropyl ether); TLC (EtOAc:hexane, 3:2 v/v): $R_f = 0.16$; $[\alpha]_D = +6$ (c = 1.2% w/v in $CHCl_3$) [lit.[19] $[\alpha]_D = -6$ (c = 1.0% w/v in $CHCl_3$) for the enantiomer]; ^1H, ^{13}C and ^{31}P NMR spectra of **15** were identical to those previously reported for the enantiomer[19]; HRMS (m/z) $[M+Na]^+$ calcd. for $C_{66}H_{67}F_3NO_{16}P_3$, 1302.3517; found 1302.3492; analysis (calcd., found for $C_{66}H_{67}F_3NO_{16}P_3$): C (61.92, 62.0), H (5.28, 5.26), N (1.09, 1.18).

L-IP$_3$ homo-dimer (8)

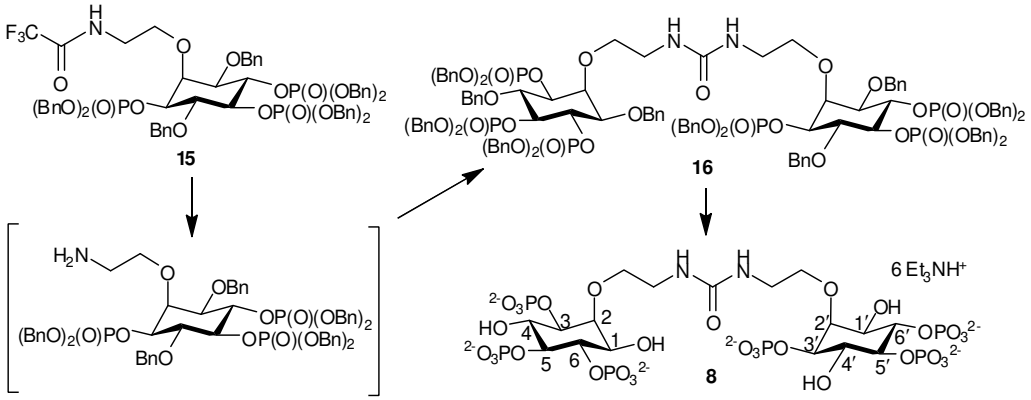

To a solution of **15** (192 mg, 0.15 mmol) in THF (3 mL) was added a solution of $LiOH.H_2O$ (63 mg, 1.5 mmol) in MeOH (3 mL) and water (1.5 mL). The mixture was stirred at room temp for 1 h, after which TLC (CH_2Cl_2:MeOH:NH_4OH, 200:20:1 v/v) showed complete conversion of starting material ($R_f = 0.90$) into the amine product ($R_f = 0.40$). The mixture was then diluted with Et_2O (30 mL) and washed with brine (20 mL). The organic layer was dried over $MgSO_4$ and concentrated (do not heat) to a volume of 1-2 mL. To this solution was added dry THF (2 mL) followed bis(4-nitrophenyl) carbonate (15.2 mg, 0.05 mmol,). The solution was stirred at room temp for 2 h under N_2, after which time TLC ($CHCl_3$:acetone, 5:1 v/v) showed a product ($R_f = 0.10$) together with 4-nitrophenol ($R_f = 0.56$), **17** ($R_f = 0.28$) and some unreacted amine ($R_f = 0$). More bis(4-nitrophenyl) carbonate (5 mg) was therefore added, and after a further 1 h, TLC now showed that only traces of unreacted amine and **17** remained. The solution was concentrated and the residue was purified by flash chromatography (EtOAc:hexane, 2:1, then 4:1 v/v, then EtOAc) to give **16** (107 mg, 0.045 mmol) as a colourless oil; TLC R_f 0.10 ($CHCl_3$/acetone 5:1); ^1H, ^{13}C and ^{31}P NMR spectra of **16** were identical to those previously reported for the enantiomer.[19] The product **16** was taken up in MeOH (30 mL) and de-ionised water (6 mL) was added, followed by $Pd(OH)_2$ on carbon (20%, 50% water, 200 mg). The mixture was shaken in a Parr hydrogenator under H_2 (50 p.s.i.) for 18 h. The catalyst was removed by filtration through a PTFE syringe filter and

Nature Chemical Biology: doi:10.1038/nchembio.195

1.0 M TEAB (1 mL) was added. The solvents were removed by evaporation under reduced pressure and the residue was purified by ion-exchange chromatography on Q-Sepharose Fast Flow resin eluting with a gradient of TEAB (0 to 2.0 moldm^{-3}), to give **8** as a colorless glass (0.033 mmol, 73% from **16**). $[\alpha]_D$ = +15 (c = 1.3% w/v in MeOH), [lit.[19] $[\alpha]_D$ for the enantiomer **2** = –14 (c = 0.4% w/v in MeOH)]; ^{1}H NMR (400 MHz, D_2O): δ 4.19 (ddd, J = 10.1, 9.8, 9.0 Hz, 2H, H-6 and H-6′), 3.98 (dd, J = 2.8, 2.8 Hz, 2H, H-2 and H-2′), 3.98–3.88 (m, 4H, H-3, H-3′, H-5 and H-5′), 3.84–3.78 (m, 4H, H-4, H-4′ and 2 × OC*H*HCH$_2$N), 3.72–3.67 (m, 2H, 2 × OCH*H*CH$_2$N), 3.63 (dd, J = 10.1, 2.8 Hz, 2H, H-1 and H-1′), ~3.2 (m, 4H, buried by TEA$^+$ CH$_2$, 2 × OCH$_2$C*H*$_2$N); ^{13}C NMR (100 MHz, D_2O): δ 160.6 (urea C=O), 79.3 (C-2 and C-2′), 78.3 (with J_{CP} couplings, C-5 and C-5′), 77.1 (with J_{CP} couplings, C-6 and C-6′), 75.3 ($^2J_{CP}$ = 5.4 Hz, C-3 and C-3′), 72.5 (2 × O*C*H$_2$CH$_2$N), 71.2 (with J_{CP} couplings, C-4 and C-4′), 70.6 (C-1 and C-1′), 40.1 (2 × OCH$_2$*C*H$_2$N); ^{31}P NMR (109 MHz, CD_3OD): δ 2.90 (2P), 2.49 (2P) and 1.44 (2P); HRMS (m/z) [M]$^-$ calcd. for $C_{17}H_{38}N_2O_{31}P_6$, 950.9806; found 950.9853.

D-1,4-di-*O*-benzyl-2-*O*-[2-(4-nitrophenyloxycarbonyl)aminoethyl]-*myo*-inositol 3,5,6-tris(dibenzylphosphate) (17)

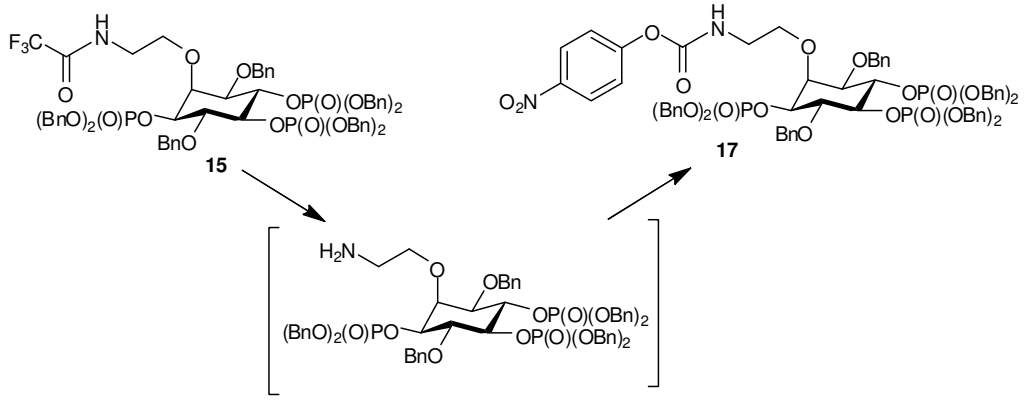

To a solution of **15** (192 mg, 0.15 mmol) in THF (3 mL) was added a solution of LiOH.H_2O (63 mg, 1.5 mmol) in MeOH (3 mL) and water (1.5 mL). The mixture was stirred at room temp for 1 h, after which TLC (CH_2Cl_2:MeOH:NH_4OH, 200:20:1 v/v) showed complete conversion of starting material (R_f = 0.90) into a more polar product (amine, R_f = 0.40). The mixture was diluted with Et_2O (30 mL) and washed with brine (20 mL). The organic layer was dried over $MgSO_4$ and concentrated (the amine product is unstable; do not heat) to a volume of 1-2 mL. To this solution was added dry THF (2 mL) and the resulting solution was added dropwise under N_2 to a solution of bis(4-nitrophenyl) carbonate (60 mg, 0.20 mmole) in dry THF (1 mL) over 10 min. The solution was stirred at room temp for 1 h under N_2, after which time TLC ($CHCl_3$:acetone, 5:1 v/v) showed a product (R_f = 0.28) together with 4-nitrophenol (R_f = 0.56), and unreacted bis(4-nitrophenyl) carbonate (R_f = 0.70). The pale yellow solution was concentrated and the residue purified by flash chromatography

Nature Chemical Biology: doi:10.1038/nchembio.195

($CHCl_3$:acetone 10:1 then 4:1 v/v) to give 4-nitrophenyl *N*-alkylcarbamate **17** (167 mg, 0.124 mmole, 83%) as a colorless oil. TLC R_f = 0.28 ($CHCl_3$/acetone 5:1); ^{1}H NMR ($CDCl_3$, 270 MHz): δ 8.09 (d, J = 9.2 Hz, 2H), 7.36–7.04 (m, 40H), 6.98 (d, J = 9.2 Hz, 2H), 6.32 (br t, J = 5.2 Hz, 1H), 5.07–4.44 (m, 1H), 4.19 (ddd, J = 9.4, 7.0, 2.4 Hz, 1H), 4.10 (br s, 1H), 4.06 (dd, J = 9.4, 8.9 Hz, 1H), 3.83–3.68 (m, 2H), 3.41 (dd, J = 9.9, 2.0 Hz, 1H), 3.38–3.28 (m, 2H); ^{13}C NMR ($CDCl_3$, 68 MHz): δ 156.2, 153.5, 144.6, 138.1, 137.0, 136.0, 135.9, 135.5, 135.4, 128.9, 128.7, 128.5, 128.4, 128.3, 128.2, 128.0, 127.9, 127.2, 125.0, 122.1, 78.9, 78.2, 78.1, 77.9, 77.8, 76.4, 74.7, 73.3, 72.3, 69.8–69.3 (overlapping CH_2 with $^2J_{CP}$ couplings), 41.7; ^{31}P NMR ($CDCl_3$, 109 MHz): δ –1.16 (1P), –1.05 (1P), –0.82 (1P); HRMS (*m*/*z*) $[M+Na]^+$ calcd. for $C_{71}H_{71}N_2O_{19}P_3$, 1371.3756; found 1371.3751.

IP$_3$–L-IP$_3$ hetero-dimer (5)

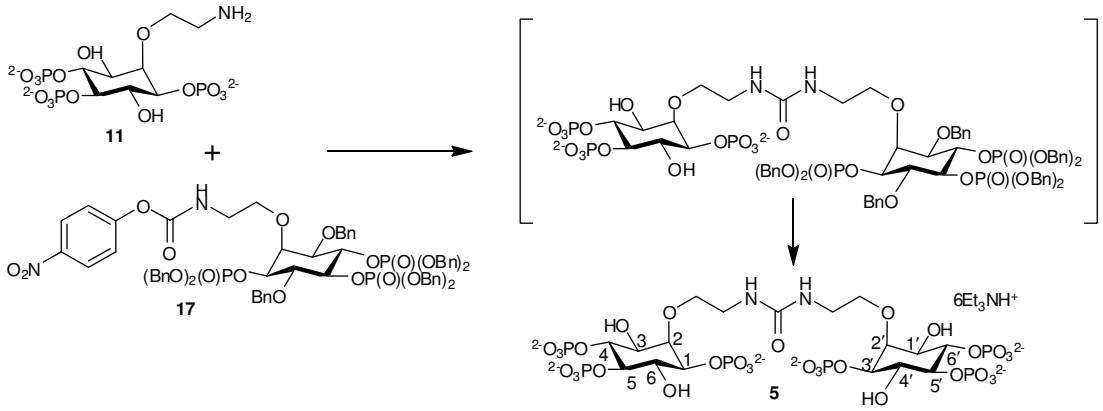

A solution of **17** (20 mg, 15 μmole) in CD_3OD (0.75 mL) was added to **11** (15 mg, 20 μmole) followed by dry triethylamine (20 μL) and a trace of EDTA. The homogeneous solution was transferred to an NMR tube and kept at room temperature. A ^{31}P NMR spectrum taken after 30 min showed that that approx. 30% of **11** had been converted into a new product and a second ^{31}P NMR spectrum taken after 5 h showed that the reaction was now 50% complete. More **17** (20 mg, 15 μmole) was added and the solution was left at room temp overnight. The next day, a ^{31}P NMR spectrum showed that the reaction was essentially complete. The yellow solution was concentrated, then taken up in deionised water (20 mL) and washed with ether (20 mL). The aqueous layer was concentrated and the residue was taken up in MeOH (20 mL) and deionised water (5 mL). $Pd(OH)_2$ on carbon (50 mg, 15-20%, 50% water) was added and the suspension was shaken in a Parr hydrogenator under H_2 (50 p.s.i.) for 16 h. The catalyst was removed by filtration through a PTFE filter, giving a colorless solution, which was neutralised by addition of aqueous TEAB (1.0 moldm^{-3}, 1 mL) and then concentrated. The residue was purified by ion-exchange chromatography on Q Sepharose Fast Flow resin eluting with a gradient of aqueous TEAB (0 to 2.0 moldm^{-3}). Two cleanly-separated phosphorus-containing fractions were collected, the first fraction containing trisphosphates. Tubes containing the second, late-eluting fraction were combined and concentrated to give hexakisphosphate **5** as a colorless glass (10.0 μmole, 50% yield). $[\alpha]_D^{20}$ = 0 (c = 0.4% w/v in

Nature Chemical Biology: doi:10.1038/nchembio.195

MeOH); ^{1}H NMR (D_2O, 400 MHz): δ 4.17 (ddd, J = 10.0, 9.8, 9.0 Hz, 2H, H-4 and H-6′), 3.95 (dd, J = 2.4, 2.4 Hz, 2H, H-2 and H-2′), 3.95–3.84 (m, 4H, H-1, H-3′, H-5 and H-5′), 3.82–3.75 (m, 4H, H-6, H-4′ and 2 × OC*H*HCH$_2$N), 3.69–3.64 (m, 2H, 2 × OCH*H*CH$_2$N), 3.60 (dd, J = 9.8, 2.8 Hz, 2H, H-3 and H-1′), ~3.2 (m, 4H, buried by TEA^+ CH_2, 2 × OCH$_2$C*H*$_2$N); ^{13}C NMR (D_2O, 100 MHz): δ 160.6 (urea C=O), 79.3 (C-2 and C-2′), 78.2 (with J_{CP} couplings, C-5 and C-5′), 77.1 (with J_{CP} couplings, C-4 and C-6′), 75.3 ($^{2}J_{CP}$ = 6.2 Hz, C-1 and C-3′), 72.6 (2 × O*C*H$_2$CH$_2$N), 71.1 (with J_{CP} couplings, C-6 and C-4′), 70.6 (C-3 and C-1′), 40.04 (2 × OCH$_2$*C*H$_2$N); ^{31}P NMR (CD_3OD, 109 MHz) δ 3.07 (2P), 2.51 (2P) and 1.57 (2P); HRMS (m/z) $[M]^-$ calcd for $C_{17}H_{38}N_2O_{31}P_6$, 950.9806; found 950.9845.

Nature Chemical Biology: doi:10.1038/nchembio.195

Syntheses of IP_3–IP_5 hetero-dimer (6) and IP_3–Ins hetero-dimer (7)

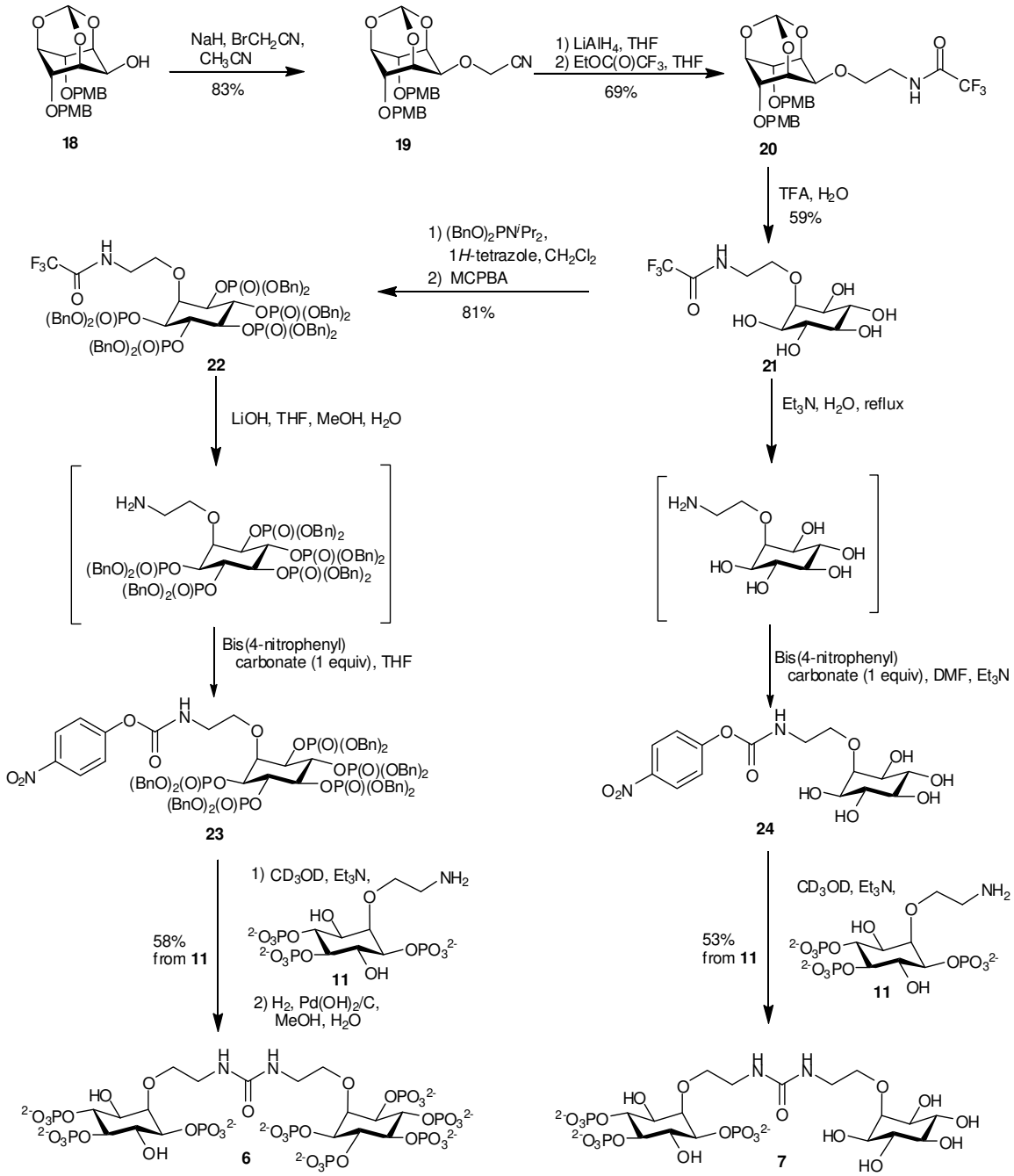

2-*O*-cyanomethyl-4,6-di-*O*-(4-methoxybenzyl)-*myo*-inositol 1,3,5-orthoformate (19)

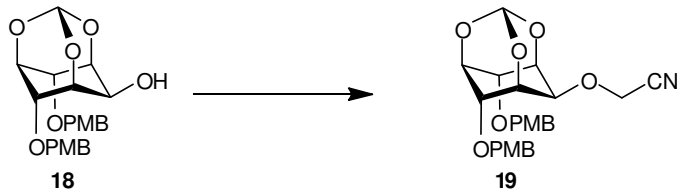

To a solution of alcohol **18**[49] (1.29 g, 3.00 mmol) in dry acetonitrile (20 mL) was added sodium hydride (600 mg of a 60% dispersion in mineral oil, 15.0 mmole). The suspension

Nature Chemical Biology: doi:10.1038/nchembio.195

was stirred under N_2 at room temperature for 1 h and then cooled to –30 ºC. Bromoacetonitrile (1.15 mL, 16.5 mmole) was added dropwise, and stirring was continued at –40 ºC to –20 ºC for 5 h. The suspension was then allowed to warm to room temperature and stirring was continued overnight. The resulting brown liquid was concentrated and the residue was suspended in water (100 mL), and extracted with Et_2O (3 × 50 mL). The combined organic extracts were dried over $MgSO_4$ and concentrated to give a brown oily residue. Purification by flash chromatography ($CHCl_3$:EtOAc, 10:1 v/v) gave the product **19** as a white solid (1.17 g, 2.49 mmol, 83 %); mp: 106.5–107.5 ºC (from ethyl acetate:hexane); TLC ($CHCl_3$:EtOAc, 5:1 v/v): R_f = 0.46; ^{1}H NMR (270 MHz, $CDCl_3$): δ 7.21 (d, J = 8.4 Hz, 4H), 6.84 (d, J = 8.4 Hz, 4H), 5.47 (d, J = 1.0 Hz, 1H), 4.62, 4.47 (AB system, J_{AB} = 11.4 Hz, 4H), 4.43–4.38 (m, 1H), 4.33 (t, J = 4.0 Hz, 2H), 4.30–4.26 (m, 2H), 4.29 (s, 2H), 4.13–4.09 (m, 1H), 3.79 (s, 6H); ^{13}C NMR (68 MHz, $CDCl_3$): δ 159.6, 123.0, 129.8, 116.4, 113.9, 103.3, 73.6, 71.8, 70.3, 69.6, 68.1, 55.4, 54.7; HRMS (m/z) $[M + Na]^+$ calcd. for $C_{25}H_{27}NO_8$ 492.1629; found 492.1632; analysis (calcd., found for $C_{25}H_{27}NO_8$): C (63.96, 63.8), H (5.80, 5.77), N (2.98, 2.82).

2-*O*-[2-(2,2,2-trifluoroacetylamino)ethyl]-4,6-di-*O*-(4-methoxybenzyl)-*myo*-inositol 1,3,5-orthoformate (20)

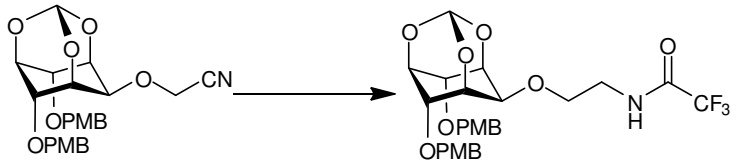

19 **20**

To a solution of $LiAlH_4$ in THF (2.5 mL of a 1 M solution, 2.5 mmol) under N_2 at room temperature was added a solution of **19** (1.17 g, 2.49 mmol) in dry THF (4 mL) dropwise over 5 min. The reaction was stirred at room temperature for 30 min and then quenched by careful addition of water. 15% aq. NaOH (50 mL) was added and the resulting solution was extracted with ether (3 × 50 mL). The combined organic extracts were dried ($MgSO_4$) and concentrated to give the crude amine as a colorless oil. The crude amine was taken up in dry THF (5 mL) and ethyl trifluoroacetate (0.5 mL, 4.2 mmol) was added. The solution was stirred at room temperature overnight and then concentrated to give an oil, which was purified by flash chromatography on silica (EtOAc:hexane, 1:3 v/v) giving **20** as a white solid (983 mg, 1.73 mmol, 69%); mp 97–99 ºC (from EtOAc:hexane); TLC (ether): R_f = 0.48; ^{1}H NMR (270 MHz, $CDCl_3$): δ 7.19 (d, J = 8.5 Hz, 4H), 6.83 (d, J = 8.4 Hz, 4H), 5.45 (d, J = 0.9 Hz, 1H), 4.62, 4.46 (AB system, J_{AB} = 11.0 Hz, 4H), 4.42–4.38 (m, 1H), 4.32 (t, J = 3.9 Hz, 2H), 4.21–4.17 (m, 2H), 3.89–3.86 (m, 1H), 3.80 (s, 6H), 3.63–3.52 (m, 4H); ^{13}C NMR (100 MHz, $CDCl_3$): δ 159.5, 157.3 ($^2J_{CF}$ = 37.6 Hz), 129.54, 129.51, 115.8 ($^1J_{CF}$ = 288 Hz), 113.9, 103.2, 73.7, 71.7, 70.1, 68.4, 68.0, 66.3, 55.3, 39.7; ^{19}F NMR (376 MHz, $CDCl_3$):

Nature Chemical Biology: doi:10.1038/nchembio.195

δ –75.9; HRMS (*m*/*z*) $[M + Na]^+$ calcd. for $C_{27}H_{30}F_3NO_9$, 592.1765; found 592.1738; analysis (calcd., found for $C_{27}H_{30}F_3NO_9$): C (56.94, 56.8), H (5.31, 5.28), N (2.46, 2.41).

2-*O*-[2-(2,2,2-trifluoroacetylamino)ethyl]-*myo*-inositol (21)

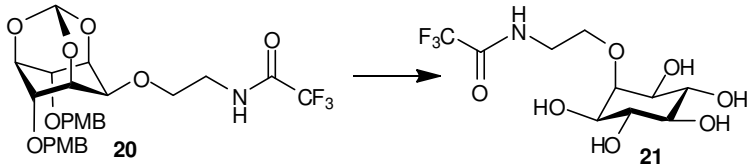

To **20** (400 mg, 0.702 mmol) was added 95% aqueous trifluoroacetic acid (5 mL). The solution was stirred at room temp for 12 h and then concentrated, leaving a solid residue. Recrystallisation from hot propan-2-ol gave **21** (132 mg, 0.413 mmole, 59%) mp: 205–208 ºC (dec); TLC (CH_2Cl_2:MeOH, 3:1 v/v): R_f = 0.20; ^{1}H NMR (270 MHz, D_2O): δ 3.90 (t, J = 5.2 Hz, 2H), 3.82 (br s, 1H), 3.61–3.48 (m, 6H), 3.19 (br t, J ~ 9 Hz, 1H, H-5); ^{1}H NMR (270 MHz, d_7-DMF) δ 9.44 (br s, 1H), 4.96 (d, J = 5.2 Hz, 2H), 4.72 (d, J = 4.1 Hz, 3H), 3.90 (t, J = 5.2 Hz, 2H), 3.76 (t, J = 2.8 Hz, 1H), 3.60–3.38 (m, 6H), 3.09 (dt, J = 3.9 Hz, 8.8 Hz, 1H); ^{13}C NMR (100 MHz, D_2O): δ 159.2 ($^2J_{CF}$ = 37.6 Hz), 116.1 ($^1J_{CF}$ = 286 Hz), 81.8, 74.6, 72.8, 71.6, 71.4, 40.5; HRMS (*m*/*z*) $[M + Na]^+$ calcd. for $C_{10}H_{16}F_3NO_7$ 342.0771; found 342.0769; analysis (calcd., found for $C_{10}H_{16}F_3NO_7$): C (37.62, 37.4), H (5.05, 5.01), N (4.39, 4.06).

2-*O*-[2-(2,2,2-trifluoroacetylamino)ethyl]-*myo*-inositol 1,3,4,5,6-pentakis(dibenzylphosphate) (22)

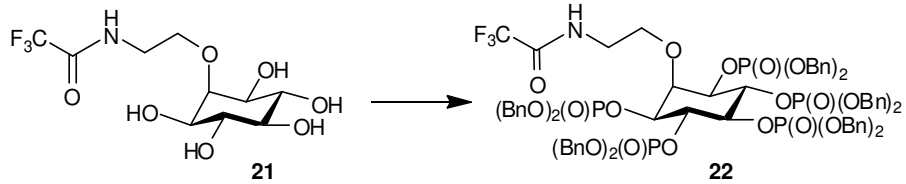

To a suspension of 1*H*-tetrazole (430 mg 6.14 mmol) and **21** (262 mg, 0.821 mmol) in dry CH_2Cl_2 (10 mL) under N_2 was added bis(benzyloxy)diisopropylaminophosphine (1.70 g, 4.93 mmol). The mixture was stirred at room temperature for 1.5 h and then cooled to –78 ºC, before MCPBA (57%, 2.5 g, 8.2 mmol) was added in portions over 1 min. The mixture was allowed to warm to room temperature and then diluted with CH_2Cl_2 (50 mL). The clear solution was washed with 10% aq. sodium metabisulfite solution (50 mL), dried over $MgSO_4$ and concentrated. The residue was purified by flash chromatography eluting with CH_2Cl_2:acetone 10:1 then 3:1 v/v to give **22** as a colorless oil (1.08 g, 0.667 mmol, 81%); TLC (CH_2Cl_2:acetone, 5:1 v/v) R_f = 0.20; ^{1}H NMR (270 MHz, $CDCl_3$): δ 7.97 (broad, 1H, amide NH), 7.27–7.11 (m, 50H), 5.06–4.87 (m, 22H), 4.50–4.37 (m, 2H), 4.24 (ddd, J = 9.5, 9.5, 2.2 Hz, 2H), 3.70 (t, J = 4.9 Hz, 2H), 3.32 (m, 2H); ^{13}C NMR (100 MHz, $CDCl_3$): δ 157.6 ($^2J_{CF}$ = 36.8 Hz, *C*(O)CF_3), 135.8–135.2 (*ipso-C* of $POCH_2$*Ph*), 128.6–127.9 (*C*H of

Nature Chemical Biology: doi:10.1038/nchembio.195

Ph), 115.9 ($^1J_{CF}$ = 288 Hz, *C*F_3), 75.9, 75.4, 75.2 and 74.6 (broad signals with J_{CP} couplings, inositol ring *C*H), 71.1 (O*C*H_2CH_2N), 69.9–69.6 (with $^3J_{CP}$ couplings, OPO*C*H_2Ph), 40.1 (OCH_2*C*H_2N); ^{19}F NMR (376 MHz, $CDCl_3$): δ –75.14; ^{31}P NMR (109 MHz, $CDCl_3$): δ –0.78 (3P), –1.37 (2P); analysis (calcd., found for $C_{80}H_{81}F_3NO_{22}P_5$): C (59.30, 57.4), H (5.04, 4.96), N (0.86, 0.85); HRMS (*m*/*z*) $[M]^-$ calcd. for $C_{80}H_{81}F_3NO_{22}P_5$ 1618.3812; found 1618.3788.

IP_3–IP_5 hetero-dimer (6)

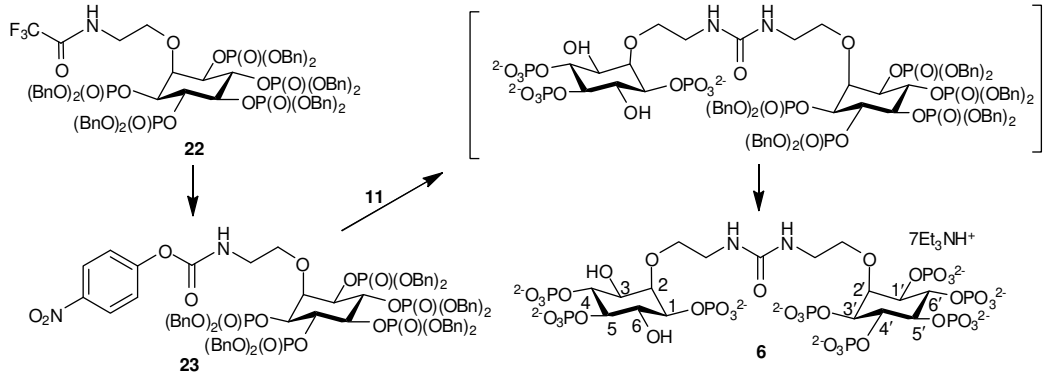

To a solution of **22** (261 mg, 0.161 mmol) in THF (4 mL) was added a solution of LiOH.H_2O (98 mg, 2.34 mmol) in MeOH (4 mL) and water (2 mL). The mixture was stirred at room temp for 1 h, after which TLC (CH_2Cl_2:MeOH:NH_4OH, 200:20:1 v/v) showed complete conversion of starting material (R_f = 0.90) into a more polar product (R_f = 0.50). The mixture was then diluted with Et_2O (40 mL) and washed with brine (20 mL). The organic layer was dried over $MgSO_4$ and concentrated* to give the crude amine as an oil (250 mg). [*Note: this step led to a low yield of **23**, probably because the solution in ether was evaporated to dryness under reduced pressure with heating, causing partial decomposition of the unstable amine. We later found that decomposition of a related intermediate (see methods for **8** and **17**) could be avoided by concentrating the solution in ether, without heating, to a volume of 1–2 mL before the next step]. Dry THF (2 mL) was added and the resulting solution of crude amine was added to a solution of bis(4-nitrophenyl) carbonate (48.7 mg, 0.160 mmole) in dry THF (1 mL) dropwise over 10 min. The solvents were evaporated and the residue was purified by flash chromatography on silica ($CHCl_3$ then $CHCl_3$:MeOH, 50:1 v/v) giving 4-nitrophenyl *N*-alkylcarbamate **23** (104 mg) as an oil, contaminated with traces of 4-nitrophenol. TLC R_f = 0.40, $CHCl_3$:MeOH 50:1 v/v; ^{1}H NMR (270 MHz, $CDCl_3$): δ 8.04 (d, J = 9.2 Hz, 2H), 7.35–7.08 (m, 52H), 6.61 (br t, 1H), 5.14–4.90 (m, 22H), 4.58 (br s, 1H), 4.41 (q, J ~ 9.4 Hz, 1H), 4.25 (dt, J = 2.0, 9.4 Hz, 2H), 3.82–3.76 (m, 2H), 3.36–3.26 (m, 2H); ^{31}P NMR (109 MHz, $CDCl_3$): δ –0.49 (2P), –0.57 (1P), –1.24 (2P). A solution of **23** (80 mg, 47 μmole) in CD_3OD was added to **11**[23] (11 mg, 15 μmole), followed by EDTA (1 mg) and dry triethylamine (15 μL). The mixture was transferred to an NMR tube and suspended in an ultrasound bath. After 1 h, a ^{31}P NMR spectrum showed that the reaction was about 40% complete. The mixture was left to stand at room temperature overnight, after which time a second ^{31}P NMR spectrum

Nature Chemical Biology: doi:10.1038/nchembio.195

showed that the reaction was essentially complete. The yellow solution was concentrated and the residue taken up in MeOH (20 mL) and deionised water (5 mL). $Pd(OH)_2$ on carbon (50 mg, 15-20%, 50% water) was added and the mixture was shaken in a Parr hydrogenator under H_2 at 50 p.s.i. for 16 h. The catalyst was removed by filtration through a PTFE filter, giving a colourless solution, which was neutralised with 1.0 moldm^{-3} TEAB and concentrated. The residue was taken up in deionised water and purified by ion-exchange chromatography on Q Sepharose Fast Flow resin eluting with a gradient of aqueous TEAB (0 to 2.0 moldm^{-3}). Two phosphorus-containing fractions eluted, the first (0.8 to 1.0 moldm^{-3} TEAB) containing a pentakisphosphate. The second fraction, containing the octakisphosphate target, was cleanly separated, eluting over 1.1 to 1.2 moldm^{-3} TEAB and concentrated to give **6** as a colorless glass (8.7 μmole, 58% from **11**). ^{1}H NMR (400 MHz, D_2O): δ 4.37 (ddd appears as br q, J ~ 10, 9, 9 Hz, 2H, H-4′ and H-6′), 4.19 (ddd appears as br q, J ~ 9, 9, 9 Hz, 1H, H-4), 4.12–4.02 (m, 4H, H-1′, H-2′, H-3′ and H-5′), 3.98 (broad s, 1H, H-2), 3.97–3.87 (m, 2H, H-1 and H-5), 3.84–3.77 (m, 4H, H-6, OC*H*CHCH$_2$N and 2 × OCH*H*CH$_2$N), 3.71–3.66 (m, 1H, OC*H*CHCH$_2$N), 3.62 (dd, J ~ 10, 3 Hz, 1H, H-3), approx. 3.2 (m, buried, 4H, OCH$_2$C*H*$_2$N); ^{1}H NMR (270 MHz, CD_3OD): δ 4.56 (ddd, J = 9.7, 9.6, 8.8 Hz, 2H, H-4′ and H-6′), 4.35 (ddd, J = 9.1, 8.9, 8.7 Hz, 1H, H-4), 4.27–3.82 (m, 12H, H-1, H-1′, H-2, H-2′, H-3′, H-5, H-5′, H-6 and 2 × OC*H*$_2$CH$_2$N), 3.61 (dd, J = 9.7, 2.0 Hz, 1H, H-3), approx. 3.3 (m, buried, 4H, OCH$_2$C*H*$_2$N); ^{13}C NMR (D_2O, 100 MHz): δ 160.5 (urea C=O), 79.5 (C-2), 78.8 (C-2′), 78.3 (with J_{CP} couplings, C-5), 77.5 (with J_{CP} couplings, C-5′), 77.1 (with J_{CP} couplings, C-4), 76.2 (with J_{CP} couplings, C-4′ and C-6′), 75.3 ($^2J_{CP}$ = 5.4 Hz, C-1), 74.1 (C-1′ and C-3′), 72.7 and 72.5 (O*C*H$_2$CH$_2$N), 71.1 (with J_{CP} couplings, C-6), 70.6 (C-3), 39.9 (2 × OCH$_2$*C*H$_2$N); ^{31}P NMR* (109 MHz, CD_3OD): δ 2.92 (1P), 2.63 (1P), 2.05 (1P), 1.80 (1P), 1.69 (1P), 1.40 (1P), 0.96 (1P), 0.86 (1P); ^{31}P NMR (109 MHz, CD_3OD, Et_3N added): δ 5.64 (1P), 4.31 (1P), 2.62 (1P), 2.40 (3P), 1.28 (2P); HRMS (*m/z*): $[M]^-$ calcd for $C_{17}H_{40}N_2O_{37}P_8$, 1110.9133; found 1110.9141. *The IP_5 moiety is desymmetrized by the linked IP_3 moiety, giving rise to eight distinct ^{31}P signals for **6** when the ^{31}P NMR spectrum is taken in CD_3OD. The ^{31}P NMR spectrum collapses to five lines on addition of Et_3N.

IP$_3$-Ins hetero-dimer (7)

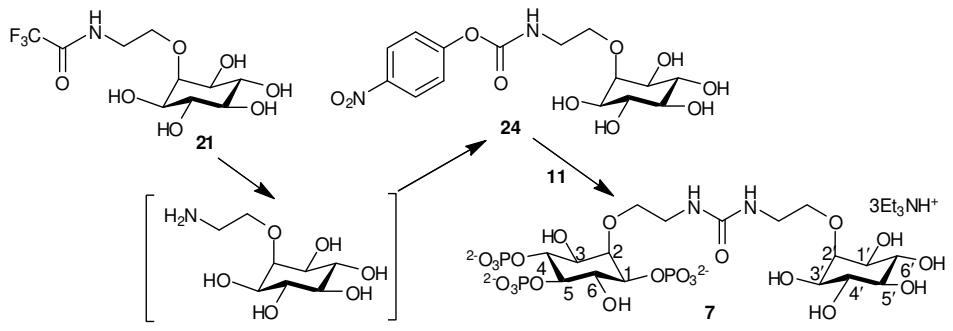

Nature Chemical Biology: doi:10.1038/nchembio.195

To a solution of **21** (319 mg, 1.00 mmole) in deionised water (10 mL) was added triethylamine (1 mL). The solution was heated at reflux for 1 h and then concentrated to dryness to give a residue, which was taken up in dry DMF (4 mL). Half of the resulting solution (2 mL) was added to a solution of bis(4-nitrophenyl) carbonate (152 mg, 0.50 mmol) in dry DMF (4 mL) dropwise over 30 min. At this stage, TLC (CH_2Cl_2:MeOH 3:1, v/v) of the colourless solution showed that unreacted bis(4-nitrophenyl) carbonate ($R_f = 0.9$) and amine ($R_f = 0$) remained. Dry triethylamine (50 μL) was added dropwise over 10 min after which time the solution was pale yellow. TLC indicated that all bis(4-nitrophenyl) carbonate had now been consumed and showed a product ($R_f = 0.22$). The solvents were removed and the residue was purified by dissolving in hot MeOH, followed by cooling and addition of $CHCl_3$ to precipitate **24** as an off-white solid (107 mg, 0.276 mmole, 55%). The 4-nitrophenyl *N*-alkylcarbamate **24** could also be purified by flash chromatography (CH_2Cl_2:MeOH, 4:1 v/v) but always contained traces of 4-nitrophenol. ^{1}H NMR (270 MHz, d_7-DMF): δ 8.29 (d, J = 9.2 Hz, 2H), 7.45 (d, J = 9.2 Hz, 2H), 4.83 (d, J = 5.5 Hz, D_2O exch., 2H), 4.75–4.66 (br m, D_2O exch., 3H), 3.89 (t, J = 5.4 Hz, 2H), 3.74 (t, J = 2.5 Hz, 1H), 3.54 (ddd, J = 9.4, 8.5, 3.0 Hz, 2H), 3.41–3.33 (m, 4H), 3.07 (td, J = 8.5 Hz, 1.7 Hz, 1H); MS: (m/z) 389.2 $[M]^+$. To a solution of **11**[23] (14.7 mg, 20 μmole) in CD_3OD in an NMR tube was added dry triethylamine (50 μL), EDTA (2 mg) and **24** (11.6 mg, 30 μmole). A ^{31}P NMR spectrum taken after 18 h showed that the reaction was not complete. Further **24** (4.0 mg, 10 μmole) was added and the NMR tube was suspended in an ultrasound bath for 1 h. A ^{31}P NMR spectrum showed that the reaction was now complete, with conversion of **11** into a single trisphosphate product. The solvents were removed and the residue was purified by ion-exchange chromatography on Q Sepharose Fast Flow resin eluting with a gradient of aqueous TEAB (0 to 1.0 moldm^{-3}) to give **7** as a colorless glass (10.6 μmole, 53% yield from **11**). ^{1}H NMR (400 MHz, D_2O): δ 4.22 (ddd, J = 9.8, 9.0, 9.0 Hz, 1H, H-4), 3.99 (br s, 1H, H-2), 3.97–3.89 (m, 2H, H-1 and H-5), 3.86–3.80 (m, 2H, 2 × OC*H*HCH$_2$N), 3.77 (dd, J = 2.7, 2.7 Hz, H-2′), 3.75–3.71 (m, 3H, H-6 and 2 × OCH*H*CH$_2$N), 3.65 (dd, J = 9.8, 2.7 Hz, 1H, H-3), 3.54 (two overlapping but slightly offset dd*, J = 9.8, 9.8 Hz, 2H, H-4′ and H-6′), 3.45 (two overlapping but slightly offset dd*, J = 9.8, 2.7 Hz, 2H, H-1′ and H-3′), 3.25–3.21 (m, 4H, 2 × OCH$_2$C*H*$_2$N), 3.12 (dd, J = 9.4, 9.0 Hz, H-5′); ^{13}C NMR (100 MHz, D_2O): δ 160.7 (urea C=O), 81.4 (C-2′), 79.3 (C-2), 78.2 (with J_{CP} couplings, C-5), 76.9 (with J_{CP} couplings, C-4), 75.2 ($^2J_{CP}$ = 5.4 Hz, C-1), 74.4 (C-5′), 73.0 and 72.7 (O*C*H$_2$CH$_2$N), 72.5 (C-4′ and C-6′), 71.52 and 71.50 (C-1′ and C-3′)*, 71.4 (with J_{CP} couplings, C-6), 70.7 (C-3), 40.1 (2 × OCH$_2$*C*H$_2$N); ^{31}P NMR (109 MHz, CD_3OD): δ 3.56 (1P), 2.53 (1P), 1.76 (1P); ^{1}HRMS (m/z): $[M]^-$ calcd for $C_{17}H_{35}N_2O_{22}P_3$, 711.0816; found 711.0884. *The inositol ring is desymmetrized by the linked IP_3 moiety.

Nature Chemical Biology: doi:10.1038/nchembio.195

Synthesis of IP_3–adamantane conjugate (9)

1-(*N*-succinimidyloxycarbonyl)adamantane (25)

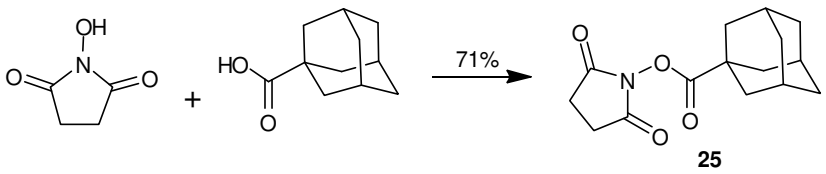

To a stirred solution of adamantane 1-carboxylic acid (1.80 g, 10.0 mmol) and *N*-hydroxysuccinimide (1.15 g, 10.0 mmol) in dry THF (20 mL) under N_2 was added a solution of DCC (2.27 g, 11.0 mmol) in dry THF (20 mL) dropwise over 15 min. A precipitate (DCU) began to appear after 10 min. Stirring was continued overnight, after which time TLC (EtOAc:hexane, 1:2 v/v) showed a major product (R_f = 0.40). The suspension was filtered through a pad of Celite, which was washed with CH_2Cl_2. The combined liquids were concentrated and the product was purified by flash chromatography (EtOAc:petrol, 1:3 v/v) to give pure **25** as a white solid (1.97 g, 7.10 mmol, 71%); crystals from CH_2Cl_2 hexane, mp: 194–196 °C; ^{1}H NMR (400 MHz, $CDCl_3$): δ 2.79 (*, 4H), 2.06 (br s, 9H), 1.74 (br s, 6 H) *This signal, corresponding to the four protons in the pyrrolidine ring, is expected to be a singlet but appears to be split into two, indicating two sets of non-equivalent protons, possibly due to restricted rotation around the bonds linking adamantane and pyrrolidine rings; ^{13}C NMR (68 MHz, $CDCl_3$): δ 172.4, 169.4, 40.5, 38.4, 36.2, 27.7, 25.7; HRMS (*m/z*): $[M+Na]^+$ calcd for $C_{15}H_{19}NO_4$, 300.1206; found 300.1202; analysis (calcd., found for $C_{15}H_{19}NO_4$): C (64.97, 64.9), H (6.91, 6.88), N (5.05, 4.93).

IP_3–adamantane conjugate (9)

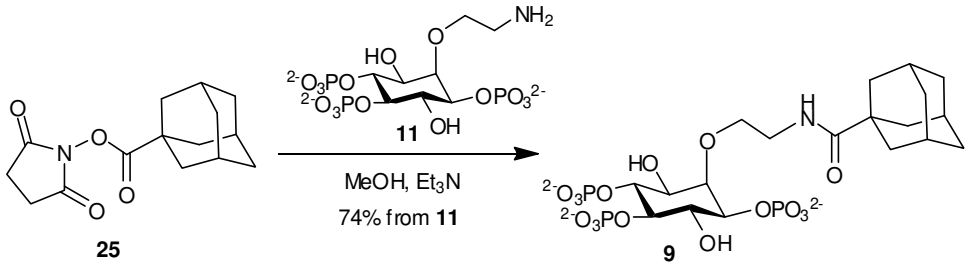

To a solution of **11**[23] (25 mg, 34 μmole) in dry MeOH (2 mL) was added **25** (18.9 mg, 68 μmole) and dry triethylamine (50 μL). The suspension was stirred at room temperature overnight. The clear solution was concentrated and a ^{31}P NMR spectrum of the residue (D_2O, EDTA and triethylamine added) showed that only around 10% of **11** had reacted (the rest was converted into the methyl ester). The solution was concentrated, redissolved in MeOH and a large excess of **25** (76 mg, 274 μmole) was added followed by further dry triethylamine (100 μL). The suspension was stirred at room temperature overnight and the resulting clear solution was concentrated. A ^{31}P NMR spectrum of the residue now showed that the reaction had progressed further, with 80 to 90% conversion of **11** into a new trisphosphate product.

Nature Chemical Biology: doi:10.1038/nchembio.195

The product was purified by ion-exchange chromatography on Q Sepharose Fast Flow resin eluting with a gradient of aqueous TEAB (0 to 1.0 moldm^{-3}). Two phosphorus-containing fractions eluted. The first contained unreacted **11**, which could be recycled, and the second contained the target trisphosphate **9,** isolated as a colorless glass (25 μmole, 74%); ^{1}H NMR (400 MHz, D_2O): δ 4.09–4.02 (m, 2H, H-2 and H-4), 3.95–3.91 (m, 1H, OC*H*HCH$_2$N), 3.85–3.66 (m, 4H, H-1, H-5, H-6 and OCH*H*CH$_2$N), 3.63 (dd, J = 10.2, 3.5 Hz, H-3), 3.37–3.33 (m, 2H, OCH$_2$C*H*$_2$N), 1.93 (br s, 3H, adamantane CH), 1.75 (br s, 6H, adamantane CH$_2$), 1.62 (br s, 6H, adamantane CH$_2$); ^{13}C NMR (D_2O, 100 MHz): δ 182.0 (amide C=O), 79.5 (C-2), 77.4 (with J_{CP} couplings, C-5), 75.4 (with J_{CP} couplings, C-4), 74.1 ($^{2}J_{CP}$ = 5.3 Hz, C-1), 72.3 (with J_{CP} couplings, C-6), 72.0 (C-3), 71.5 (O*C*H$_2$CH$_2$N), 40.6 (adamantane), 39.6 (OCH$_2$*C*H$_2$N), 38.2 (adamantane), 35.8 (adamantane), 27.7 (adamantane); ^{31}P NMR (109 MHz, D_2O, Et_3N added): δ 5.31 (1P), 5.08 (1P), 3.61 (1P); HRMS (*m/z*): [M]$^{-}$ calcd. for $C_{19}H_{34}NO_{16}P_3$, 624.1012; found 624.1008.

SUPPLEMENTARY REFERENCES

51. Nikiforovich, G.V., Leonova, V.I., Galaktionov, S.G. & Chipens, G.I. Theoretical conformational analysis of oxytocin molecule. *Int. J. Pep. Prot. Res.* **13**, 363-373 (1979).
52. Nemethy, G. *et al.* Energy parameters in polypeptides. 10. Improved gemoetrical parameters and nonbonded interactions for use in the ECEPP/3 algorithm, with application to proline-containing peptides. *J. Phys. Chem.* **96**, 6472-6484 (1992).
53. Nemethy, G., Pottle, M.S. & Scheraga, H.A. Energy parameters in polypeptides. 9. Updating of geometrical parameters, nonbonded interactions, and hydrogen bond interactions for the naturally occurring amino acids. *J. Phys. Chem.* **87**, 1883-1887 (1983).
54. Colquhoun, D. & Sigworth, F.J. Fitting and statistical analysis of single channel records. in *Single-Channel Recording* (eds. Sakmann, B. & Neher, E.) pp. 483-587 Plenum Press, New York (1995).
55. Lampe, D., Liu, C.S. & Potter, B.V.L. Synthesis of selective non-Ca^{2+}-mobilizing inhibitors of D-myo-inositol 1,4,5-trisphosphate 5-phosphatase. *J. Med. Chem.* **37**, 907-912 (1994).
56. Ames, B.N. & Dubin, D.T. The role of polyamines in the neutralization of bacteriophage deoxyribonucleic acid. *J. Biol. Chem.* **235**, 769-775 (1960).

Nature Chemical Biology: doi:10.1038/nchembio.195